cones (Fig. 6). C terminus of CaD, but not N terminus, was required for both functions. C terminus contains some actin binding domains, which are necessary for stabilization of actin bundles (7, 8), and the filopodia-like protrusion were composed of concentrated actin filaments (Fig. 1*H*). These indicate that actin stabilization by the C-terminal domains facilitates formation of these filopodial protrusions independently of N-terminal myosin binding domain.

Results of our experiments using myosin II ATPase inhibitor blebbistatin strongly suggest an inhibitory effect of N-CaD on myosin II function in hippocampal neurons and non-neuronal A549 cells (Figs. 5 and 7). However, previous *in vitro* study showed that the CaD^{1-597} fragment, which lacks the C-terminal actin-binding domains, does not inhibit actin-activated myosin ATPase activity (29). Velaz *et al.* (22) reported that CaD inhibits actin-activated myosin ATPase activity via its C-terminal F-actin-binding domains, by preventing the myosin head from binding to actin *in vitro* (21). Considering the discrepancy between these *in vitro* studies and our *in vivo* study, we propose that N-CaD inhibits myosin II function by unknown mechanisms, which may include interacting with or recruiting additional myosin-inhibitory factors. Further investigations are required to clarify how N-CaD inhibits myosin II function.

Growing evidences indicate that myosin II function is important for axon outgrowth and axon guidance (30–35). However, the molecular mechanism underlying actomyosin-mediated axon extension has not been fully evaluated. An early study by Letourneau *et al.* (36) clearly demonstrated that both "push" by microtubules and "pull" by actomyosin in the growth cone play central roles in axon extension. Actually, actin destabilization by cytochalasin D or ADF/cofilin and myosin II inhibition by blebbistatin enhance axon extension (Refs. 5, 25 and the present study). CaD may inhibit the traction force generated by the actomyosin contraction, thereby augmenting the pushing force from microtubule extension.

REFERENCES

1. Poulain, F. E., and Sobel, A. (2010) The microtubule network and neuronal morphogenesis: Dynamic and coordinated orchestration through multiple players. *Mol. Cell. Neurosci.* **43**, 15–32
2. Kwiatkowski, A. V., Rubinson, D. A., Dent, E. W., Edward van Veen, J., Leslie, J. D., Zhang, J., Mebane, L. M., Philippar, U., Pinheiro, E. M., Burds, A. A., Bronson, R. T., Mori, S., Fässler, R., and Gertler, F. B. (2007) Ena/VASP Is required for neuritogenesis in the developing cortex. *Neuron* **56**, 441–455
3. Garvalov, B. K., Flynn, K. C., Neukirchen, D., Meyn, L., Teusch, N., Wu, X., Brakebusch, C., Bamburg, J. R., and Bradke, F. (2007) Cdc42 regulates cofilin during the establishment of neuronal polarity. *J. Neurosci.* **27**, 13117–13129
4. Strasser, G. A., Rahim, N. A., VanderWaal, K. E., Gertler, F. B., and Lanier, L. M. (2004) Arp2/3 is a negative regulator of growth cone translocation. *Neuron* **43**, 81–94
5. Bradke, F., and Dotti, C. G. (1999) The role of local actin instability in axon formation. *Science* **283**, 1931–1934
6. Sobue, K., Muramoto, Y., Fujita, M., and Kakiuchi, S. (1981) Purification of a calmodulin-binding protein from chicken gizzard that interacts with F-actin. *Proc. Natl. Acad. Sci. U.S.A.* **78**, 5652–5655
7. Sobue, K., and Sellers, J. R. (1991) Caldesmon, a novel regulatory protein in smooth muscle and nonmuscle actomyosin systems. *J. Biol. Chem.* **266**, 12115–12118
8. Mayanagi, T., and Sobue, K. (2011) Diversification of caldesmon-linked actin cytoskeleton in cell motility. *Cell. Adh. Migr.* **5**, 150–159
9. Sobue, K., Morimoto, K., Inui, M., Kanda, K., and Kakiuchi, S. (1982) *Biomed. Res.* **3**, 188–196
10. Ngai, P. K., and Walsh, M. P. (1984) Inhibition of smooth muscle actin-activated myosin Mg^{2+}-ATPase activity by caldesmon. *J. Biol. Chem.* **259**, 13656–13659
11. Sobue, K., Takahashi, K., and Wakabayashi, I. (1985) Caldesmon150 regulates the tropomyosin-enhanced actin-myosin interaction in gizzard smooth muscle. *Biochem. Biophys. Res. Commun.* **132**, 645–651
12. Ishikawa, R., Yamashiro, S., and Matsumura, F. (1989) Differential modulation of actin-severing activity of gelsolin by multiple isoforms of cultured rat cell tropomyosin. Potentiation of protective ability of tropomyosins by 83-kDa nonmuscle caldesmon. *J. Biol. Chem.* **264**, 7490–7497
13. Yamashiro, S., Chern, H., Yamakita, Y., and Matsumura, F. (2001) Mutant Caldesmon lacking cdc2 phosphorylation sites delays M-phase entry and inhibits cytokinesis. *Mol. Biol. Cell* **12**, 239–250
14. Fukumoto, K., Morita, T., Mayanagi, T., Tanokashira, D., Yoshida, T., Sakai, A., and Sobue, K. (2009) Detrimental effects of glucocorticoids on neuronal migration during brain development. *Mol. Psychiatry* **14**, 1119–1131
15. Sobue, K., and Fukumoto, K. (2010) Caldesmon, an actin-linked regulatory protein, comes across glucocorticoids. *Cell Adh. Migr.* **4**, 185–189
16. Kira, M., Tanaka, J., and Sobue, K. (1995) Caldesmon and low Mr isoform of tropomyosin are localized in neuronal growth cones. *J. Neurosci. Res.* **40**, 294–305
17. Tanaka, J., Watanabe, T., Nakamura, N., and Sobue, K. (1993) Morphological and biochemical analyses of contractile proteins (actin, myosin, caldesmon and tropomyosin) in normal and transformed cells. *J. Cell Sci.* **104**, 595–606
18. Jiang, M., and Chen, G. (2006) High Ca^{2+}-phosphate transfection efficiency in low-density neuronal cultures. *Nat. Protoc.* **1**, 695–700
19. Riedl, J., Crevenna, A. H., Kessenbrock, K., Yu, J. H., Neukirchen, D., Bista, M., Bradke, F., Jenne, D., Holak, T. A., Werb, Z., Sixt, M., and Wedlich-Soldner, R. (2008) Lifeact: a versatile marker to visualize F-actin. *Nat. Methods* **5**, 605–607
20. Morita, T., Mayanagi, T., Yoshio, T., and Sobue, K. (2007) Changes in the balance between caldesmon regulated by p21-activated kinases and the Arp2/3 complex govern podosome formation. *J. Biol. Chem.* **282**, 8454–8463
21. Ray, J., Peterson, D. A., Schinstine, M., and Gage, F. H. (1993) Proliferation, differentiation, and long-term culture of primary hippocampal neurons. *Proc. Natl. Acad. Sci. U.S.A.* **90**, 3602–3606
22. Velaz, L., Ingraham, R. H., and Chalovich, J. M. (1990) Dissociation of the effect of caldesmon on the ATPase activity and on the binding of smooth heavy meromyosin to actin by partial digestion of caldesmon. *J. Biol. Chem.* **265**, 2929–2934
23. Hemric, M. E., and Chalovich, J. M. (1988) Effect of caldesmon on the ATPase activity and the binding of smooth and skeletal myosin subfragments to actin. *J. Biol. Chem.* **263**, 1878–1885
24. Li, Y., Zhuang, S., Guo, H., Mabuchi, K., Lu, R. C., and Wang, C. A. (2000) The major myosin-binding site of caldesmon resides near its N-terminal extreme. *J. Biol. Chem.* **275**, 10989–10994
25. Kuhn, T. B., Meberg, P. J., Brown, M. D., Bernstein, B. W., Minamide, L. S., Jensen, J. R., Okada, K., Soda, E. A., and Bamburg, J. R. (2000) Regulating actin dynamics in neuronal growth cones by ADF/cofilin and rho family GTPases. *J. Neurobiol.* **44**, 126–144
26. Warren, K. S., Lin, J. L., Wamblodt, D. D., and Lin, J. J. (1994) Overexpression of human fibroblast caldesmon fragment containing actin-, Ca^{++}/calmodulin-, and tropomyosin-binding domains stabilizes endogenous tropomyosin and microfilaments. *J. Cell Biol.* **125**, 359–368
27. Hayashi, K., Fujio, Y., Kato, I., and Sobue, K. (1991) Structural and functional relationships between h- and l-caldesmons. *J. Biol. Chem.* **266**, 355–361
28. Li, Y., Lin, J. L., Reiter, R. S., Daniels, K., Soll, D. R., and Lin, J. J. (2004) Caldesmon mutant defective in Ca(2+)-calmodulin binding interferes with assembly of stress fibers and affects cell morphology, growth, and motility. *J. Cell Sci.* **117**, 3593–3604
29. Wang, Z., Jiang, H., Yang, Z. Q., and Chacko, S. (1997) Both N-terminal myosin-binding and C-terminal actin-binding sites on smooth muscle

caldesmon are required for caldesmon-mediated inhibition of actin filament velocity. *Proc. Natl. Acad. Sci. U.S.A.* **94,** 11899–11904
30. Chantler, P. D., and Wylie, S. R. (2003) Elucidation of the separate roles of myosins IIA and IIB during neurite outgrowth, adhesion and retraction. *IEE Proc. Nanobiotechnol.* **150,** 111–125
31. Turney, S. G., and Bridgman, P. C. (2005) Laminin stimulates and guides axonal outgrowth via growth cone myosin II activity. *Nat. Neurosci.* **8,** 717–719
32. Loudon, R. P., Silver, L. D., Yee, H. F., Jr., and Gallo, G. (2006) RhoA-kinase and myosin II are required for the maintenance of growth cone polarity and guidance by nerve growth factor. *J. Neurobiol.* **66,** 847–867
33. Rösner, H., Möller, W., Wassermann, T., Mihatsch, J., and Blum, M. (2007) Attenuation of actinomyosinII contractile activity in growth cones accelerates filopodia-guided and microtubule-based neurite elongation. *Brain Res.* **1176,** 1–10
34. Bridgman, P. C. (2009) Myosin motor proteins in the cell biology of axons and other neuronal compartments. *Results Probl. Cell Differ.* **48,** 91–105
35. Hur, E. M., Yang, I. H., Kim, D. H., Byun, J., Saijilafu, Xu, W. L., Nicovich, P. R., Cheong, R., Levchenko, A., Thakor, N., and Zhou, F. Q. (2011) Engineering neuronal growth cones to promote axon regeneration over inhibitory molecules. *Proc. Natl. Acad. Sci. U.S.A.* **108,** 5057–5062
36. Letourneau, P. C., Shattuck, T. A., and Ressler, A. H. (1987) "Pull" and "push" in neurite elongation: observations on the effects of different concentrations of cytochalasin B and taxol. *Cell Motil. Cytoskeleton* **8,** 193–209

Original Paper

Cerebrovascular Diseases

Cerebrovasc Dis 2012;33:354–361
DOI: 10.1159/000335836

Received: August 7, 2011
Accepted: December 12, 2011
Published online: March 14, 2012

Effect of Combination Therapy with the Angiotensin Receptor Blocker Losartan plus Hydrochlorothiazide on Brain Perfusion in Patients with both Hypertension and Cerebral Hemodynamic Impairment due to Symptomatic Chronic Major Cerebral Artery Steno-Occlusive Disease: A SPECT Study

Hiroaki Saura[a, b] Kuniaki Ogasawara[a, b] Taro Suzuki[a, b] Hiroki Kuroda[a, b] Takeshi Yamashita[a, b] Masakazu Kobayashi[a, b] Kazunori Terasaki[b] Akira Ogawa[a, b]

[a]Department of Neurosurgery and [b]Cyclotron Research Center, Iwate Medical University, Morioka, Japan

Key Words
Hypertension · Angiotensin receptor blocker · Hydrochlorothiazide · Cerebral blood flow · Cerebrovascular reactivity

Abstract
Background: While the combination of an angiotensin receptor blocker with thiazide diuretics produces a clinically beneficial reduction in blood pressure in patients who otherwise only partially respond to monotherapy with an angiotensin receptor blocker, blood pressure-lowering therapy with combination antihypertensive drug regimens in patients with cerebral hemodynamic impairment may adversely affect cerebral hemodynamics. The purpose of the present exploratory study was to determine whether blood pressure-lowering therapy with the combination of the angiotensin receptor blocker losartan plus hydrochlorothiazide (LPH) worsens brain perfusion in patients with both hypertension and cerebral hemodynamic impairment due to symptomatic chronic major cerebral artery steno-occlusive disease. ***Methods:*** Patients with losartan-resistant hypertension and reduced cerebrovascular reactivity (CVR) to acetazolamide due to symptomatic chronic internal carotid artery (ICA) or middle cerebral artery (MCA) steno-occlusive disease were prospectively entered into the present study and received 50 mg/day of losartan plus 12.5 mg/day of hydrochlorothiazideat 14 weeks after the last ischemic event. Cerebral blood flow (CBF) and CVR were measured before and 12 weeks after initiating LPH using N-isopropyl-*p*-[^{123}I]-iodoamphetamine single-photon emission computed tomography (SPECT). A region of interest (ROI) was automatically placed in the MCA territory on each SPECT image using a three-dimensional stereotactic ROI template. ***Results:*** None of the 18 patients who participated in the study experienced any new neurological symptoms or adverse effects related to antihypertensive drugs. Systolic ($p < 0.001$) and diastolic ($p < 0.001$) blood pressures were significantly reduced after the administration of LPH, with average reductions of 11 mm Hg in systolic blood pressure and 10 mm Hg

KARGER

Fax +41 61 306 12 34
E-Mail karger@karger.ch
www.karger.com

1015–9770/12/0334–0354$38.00/0

Accessible online at:
www.karger.com/ced

Kuniaki Ogasawara, MD
Department of Neurosurgery, Iwate Medical University
19-1 Uchimaru
Morioka 020-8505 (Japan)
Tel. +81 19 651 5111, E-Mail kuogasa@iwate-med.ac.jp

in diastolic blood pressure. While in the affected hemisphere CBF did not differ between measurements taken before and after the administration of LPH, CVR was significantly higher after the administration of LPH than before ($p = 0.007$) and was significantly improved in 5 of 18 patients. In the contralateral hemisphere, CBF and CVR did not differ between measurements taken before and after the administration of LPH. There were no patients who experienced a significant deterioration in CBF or CVR in the affected or contralateral hemisphere after the administration of LPH. ***Conclusions:*** Although the present study was exploratory and its results were preliminary due to the small sample size, the current data suggest that blood pressure-lowering therapy with LPH apparently does not result in worsening of cerebral hemodynamics in patients with both hypertension and cerebral hemodynamic impairment due to symptomatic chronic ICA or MCA steno-occlusive disease.

Introduction

When the target blood pressure of patients with hypertension is not achieved with one antihypertensive drug, multidrug therapy should be considered [1]. In fact, multidrug therapy often produces greater blood pressure reduction at lower doses of the component agents [1].

Angiotensin receptor blockers inhibit vascular tone maintained by locally produced angiotensin II, resulting in vasodilatation of large cerebral arteries [2]. Further, pretreatment with an angiotensin receptor blocker protected hypertensive rats from brain ischemia by normalizing the cerebral blood flow (CBF) response [2], and a 4-week treatment course with this agent increased CBF in patients with a history of stroke [3]. In contrast, thiazide-type antihypertensive drugs induce diuresis, and oral long-term administration of these drugs may lead to dehydration and affect blood rheology. Treatment with hydrochlorothiazide decreases cardiac output by reducing extracellular fluid volume and plasma volume [4] and increases whole blood viscosity and hematocrit [5–8], which may reduce brain perfusion. However, the effect of combination therapy with an angiotensin receptor blocker plus a thiazide-type antihypertensive drug on brain perfusion remains unknown.

Among patients with symptomatic major cerebral artery occlusive disease, the subgroup of those with cerebral hemodynamic impairment is at increased risk of recurrent ischemic strokes [9]. Studies have demonstrated that patients with reduced cerebrovascular reactivity (CVR) to acetazolamide measured by single-photon emission computed tomography (SPECT) show an increased risk of a subsequent stroke [10, 11]. In patients with both hypertension and cerebral hemodynamic impairment, blood pressure-lowering therapy with an angiotensin receptor blocker plus a thiazide-type antihypertensive drug may adversely affect cerebral hemodynamics, facilitating the development of ischemic stroke.

The purpose of the present exploratory study was to determine whether blood pressure-lowering therapy with the combination of the angiotensin receptor blocker losartan plus hydrochlorothiazide (LPH) worsens brain perfusion in patients with both hypertension and cerebral hemodynamic impairment due to symptomatic chronic internal carotid (ICA) or middle cerebral artery (MCA) occlusion.

Methods

Patients

The study prospectively enrolled patients who satisfied the following criteria: age >20 years; carotid artery territory ischemic symptom within the last 2 months before presentation to our department; useful residual function (modified Rankin disability scale 0 or 1); unilateral or bilateral ICA or MCA atherosclerotic stenosis (≧70%) or occlusion on magnetic resonance angiography or angiography with arterial catheterization; losartan-resistant hypertension and moderately reduced CVR defined by criteria described below. Exclusion criteria were: pregnancy or breast-feeding; angina pectoris or myocardial infarction within 6 months before presentation to our department; congestive heart failure (New York Heart Association class 3/4); stenosis of the bilateral or unilateral renal arteries; serum creatinine >2.0 mg/dl, and aspartate aminotransferase >90 IU/l and/or alanine aminotransferase >80 IU/l.

A local ethics committee approved the study protocol. Written informed consent was obtained from all subjects prior to enrollment in the study.

Management and Medications

Upon the patient's presentation to our outpatient department, a physician or a nurse measured his/her blood pressure twice consecutively using the auscultatory method with a mercury sphygmomanometer while the patient was in the sitting position after a rest of at least 2 min. Blood pressure was defined as the average of the two measurements.

No antihypertensive drugs were given to patients within 8 weeks after the last cerebral ischemic event. When systolic or diastolic blood pressure 8 weeks after the last cerebral ischemic event was >140 or >90 mm Hg, respectively, patients received 25 mg/day of losartan; when the systolic or diastolic blood pressure at 2 weeks after initiating the administration of losartan was above the target value, patients received 50 mg/day of losartan; when the systolic or diastolic blood pressure at 4 weeks after initiating the dose escalation of losartan was still above the target value, pa-

tients were defined as having losartan-resistant hypertension and received 50 mg/day of losartan plus 12.5 mg/day of hydrochlorothiazide (LPH) (Preminent®).

During the study period, all patients received antiplatelet drugs such as aspirin (100 mg/day) or clopidogrel (75 mg/day).

Patients visited our outpatient clinic at 2-week intervals until 12 weeks after initiating the administration of LPH. At these visits, clinicians determined whether new neurological symptoms developed, and blood pressure was measured.

Measurement of Brain Perfusion Using SPECT

Brain perfusion was assessed using [^{123}I]N-isopropyl-*p*-iodoamphetamine (IMP) and SPECT. The IMP SPECT studies, including measurements at the resting state and with acetazolamide challenge, were performed as described previously [12]. Studies were performed twice: the day before initiating the administration of LPH and 3 months later. The CBF images were calculated according to the IMP autoradiography method [12, 13].

All SPECT images were transformed into the standard brain size and shape by linear and nonlinear transformation using SPM99 for anatomic standardization [14]. Thus, the brain images of all patients had the same anatomic format. Next, 318 constant regions of interest (ROIs) were automatically placed in both the cerebral and cerebellar hemispheres using a 3D stereotaxic ROI template [15]. The ROIs were grouped into 10 segments (callosomarginal, pericallosal, precentral, central, parietal, angular, temporal, posterior, hippocampus and cerebellum) in each hemisphere according to the arterial supply. Only 5 (precentral, central, parietal, angular and temporal) of these 10 segments were combined and defined as a ROI perfused by the MCA (fig. 1). The mean CBF value at the resting state and with an acetazolamide challenge in all pixels in the MCA ROI was calculated in each hemisphere. Then, CVR to acetazolamide was calculated as follows: CVR (%) = [(acetazolamide challenge CBF – resting CBF)/resting CBF]/100.

Using the same method, 10 normal subjects (8 men and 2 women; age, 35–65 years; mean age, 52.3 years) were studied twice at an interval of 3 months to obtain control values. For the first study, the means ± standard deviations (SDs) of CBF and CVR in the MCA ROI were 35.9 ± 4.4 ml/100 g/min and 36.8 ± 9.2%, respectively. When CVR in the MCA ROI of a patient was between the mean – 2SD (i.e. 18.4%) and the mean – 3SD (i.e. 9.2%) of the control value, it was rated as moderately reduced CVR; when CVR was ≤ the mean – 3SD, it was rated as severely reduced. Patients with moderately reduced CVR participated in the present study.

Differences between values obtained at the two studies (the second study – the first study) in the normal subjects were also calculated: 0.1 ± 4.5 ml/100 g/min for CBF and 1.1 ± 6.3% for CVR. When the difference between CBF or CVR obtained at the two studies (the second study – the first study) in a patient was ≥2SD above the mean control difference obtained from normal subjects (i.e. 9.1 ml/100 g/min for CBF; 13.7% for CVR), the patient was rated as having improved CBF or CVR, respectively; when the difference in a patient was ≤2SD below the mean control difference obtained from normal subjects (i.e. –8.9 ml/100 g/min for CBF; –11.5% for CVR), the patient was rated as having deteriorated CBF or CVR, respectively; when the difference in a patient was between 2SD above and below the mean control difference obtained from normal subjects, the patient was rated as having unchanged CBF or CVR, respectively.

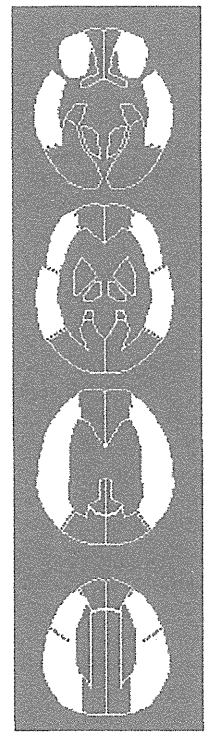

Fig. 1. Diagrams showing the ROIs of a three-dimensional stereotaxic ROI template. The white ROIs (precentral, central, parietal, angular, and temporal segments) indicate territories perfused by the bilateral MCAs.

Statistical Analysis

Because the present study was an exploratory trial, the required sample size could not be definitely estimated. Data are expressed as means ± SDs. Differences between blood pressure, CBF or CVR before and 12 weeks after initiating the administration of LPH were evaluated using the Wilcoxon signed-rank test. When there were patients with improved or deteriorated CBF or CVR, each variable was compared between patients with and without such a condition using the Mann-Whitney U test or Fisher's exact test. A multivariate statistical analysis of factors related to such a condition was also performed using a logistic regression model. In addition to variables with $p < 0.2$ in the univariate analyses, age and gender were selected for analysis in the final model. Statistical significance was set at the $p < 0.05$ level.

Results

During 30 months, 19 patients satisfied the inclusion criteria. Of these 19 patients, 1 had experienced angina pectoris within 6 months before presentation to our department and was excluded from the present study. Written informed consent was obtained from the remaining 18 patients, who ultimately entered into the present study. The characteristics of these 18 patients are summarized in table 1.

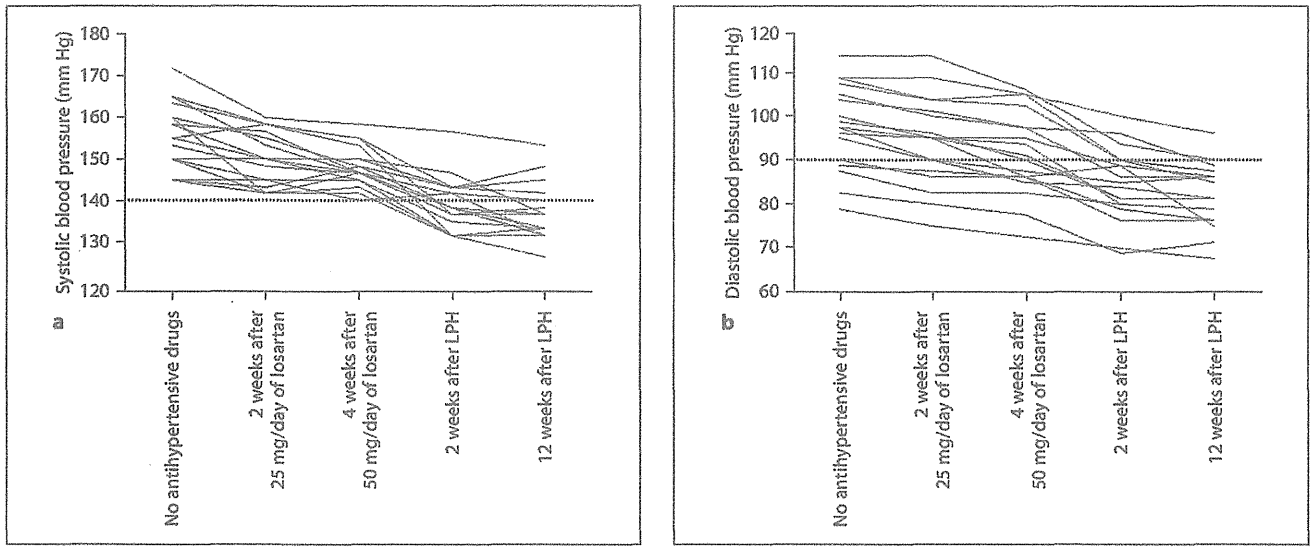

Fig. 2. Systolic (a) and diastolic (b) blood pressure values at each time point. Dashed horizontal line denotes a target value.

Table 1. Patient characteristics

Age	Gender	Body mass index	Current smoking	Excessive drinking	Diabetes mellitus	Dyslipidemia	Symptoms	Lesions on MRI	Lesions on angiography	Antiplatelet drug
67	M	26.9	yes	no	yes	yes	MCS	border zone INF	right ICA stn	CP
47	M	25.3	no	no	no	no	TIA	none	right MCA stn	AS
58	M	21.4	no	no	no	no	TIA	none	left ICA occl	CP
61	M	24.3	no	no	no	no	TIA	none	left ICA stn	AS
68	M	27.6	no	yes	no	yes	MCS	border zone INF	left ICA occl	CP
56	F	20.4	yes	no	yes	no	TIA	border zone INF	left MCA occl	AS
76	M	22.9	no	no	no	no	MCS	border zone INF	left ICA occl	CP
55	M	25.3	no	no	no	no	TIA	none	right MCA stn	AS
65	M	25.9	yes	no	yes	yes	MCS	border zone INF	left MCA occl	CP
48	M	27.3	no	no	no	no	TIA	border zone INF	right MCA occl	AS
57	M	23.6	no	no	no	yes	TIA	none	left ICA occl	AS
68	F	26.0	yes	no	no	no	MCS	border zone INF	left ICA occl	CP
55	F	22.7	no	no	no	no	TIA	none	left MCA occl	AS
65	M	22.2	no	no	no	no	TIA	none	right MCA occl	CP
48	M	26.4	no	no	yes	yes	TIA	none	left MCA occl	AS
72	M	22.5	yes	no	no	no	MCS	border zone INF	right ICA occl	CP
70	M	26.9	yes	no	no	yes	MCS	border zone INF	right ICA occl	AS
62	M	27.1	no	no	no	no	MCS	border zone INF	left ICA ocl	CP

Excessive drinking is defined as drinking alcohol >60 g/day. MRI = Magnetic resonance imaging; MCS = minor complete stroke; TIA = transient ischemic attack; INF = infarction; stn = stenosis; occl = occlusion; CP = clopidogrel; AS = aspirin.

All these 18 patients were followed up until 12 weeks after initiating the administration of LPH. All the patients also received antihypertensive drugs and underwent brain perfusion SPECT studies during the study period. None of the 18 patients experienced new neurological symptoms or adverse effects related to antihypertensive drugs.

Time courses of systolic and diastolic blood pressures for each patient are shown in figure 2. Systolic ($p < 0.001$)

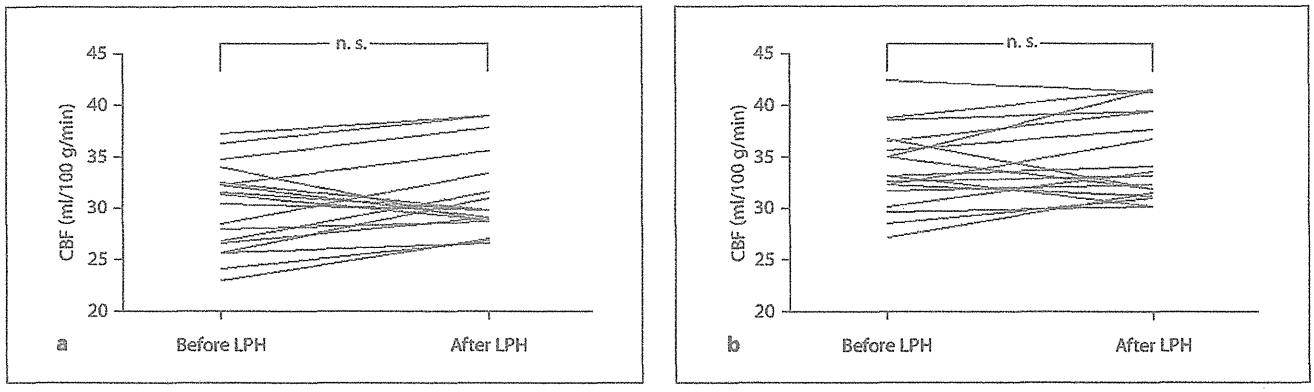

Fig. 3. Change in CBF in the affected (**a**) and contralateral (**b**) MCA territories before and after initiating the administration of LPH.

and diastolic ($p < 0.001$) blood pressures were significantly lower at 12 weeks after initiating the administration of LPH (138 ± 7 mm Hg for systolic blood pressure; 82 ± 7 mm Hg for diastolic blood pressure) than before the administration of LPH (149 ± 5 mm Hg for systolic blood pressure; 92 ± 10 mm Hg for diastolic blood pressure), respectively. Differences between values before and after the administration of LPH (values after administration – values before administration) ranged from 5 to 18 mm Hg for systolic blood pressure (11 ± 4 mm Hg) and from 2 to 18 mm Hg for diastolic blood pressure (10 ± 5 mm Hg).

CBF did not differ between measurements taken before and after the administration of LPH in the affected hemisphere (30.0 ± 4.2 ml/100 g/min before administration; 31.1 ± 4.1 ml/100 g/min after administration) or in the contralateral hemisphere (33.9 ± 3.9 ml/100 g/min before administration; 35.0 ± 4.3 ml/100 g/min after administration) (fig. 3). When based on differences between CBF before and after the administration of LPH, all patients studied were rated as having unchanged CBF in the affected and contralateral hemispheres.

While CVR in the affected hemisphere was significantly higher after the administration of LPH (23.6 ± 12.0%) than before (14.5 ± 2.3%) ($p = 0.007$), CVR in the contralateral hemisphere did not differ between these two measurements (40.0 ± 11.1% before administration; 41.7 ± 10.2% after administration) (fig. 4). When based on differences between CVR before and after the administration of LPH, in the affected hemisphere, 5 and 13 patients were rated as having improved and unchanged CVR, respectively. In the contralateral hemisphere, all patients were rated as having unchanged CVR. None of the patients were rated as having deteriorated CVR in the affected or contralateral hemisphere.

The results of the univariate analysis of factors related to improved CVR in the affected hemisphere are summarized in table 2. None of the variables, including blood pressure difference, were significantly associated with improved CVR. The following confounders were also adopted in the logistic regression model for the multivariate analysis: age, gender and site of lesion on angiography. The analysis revealed that none of the variables were significantly associated with improved CVR (table 2).

Figure 5 shows brain perfusion SPECT images in the resting state and with acetazolamide challenge before and 12 weeks after initiating the administration of LPH in patient 3.

Discussion

The present exploratory study suggests that blood pressure-lowering therapy with LPH does apparently not result in worsening of cerebral hemodynamics in patients with both hypertension and cerebral hemodynamic impairment due to symptomatic chronic ICA or MCA steno-occlusive disease.

Losartan is the first nonpeptide angiotensin II receptor antagonist studied in large clinical trials of patients with hypertension and diabetic nephropathy or left-ventricular hypertrophy [16, 17]. LPH produces a clinically beneficial reduction in blood pressure in patients who otherwise only partially respond to losartan monotherapy [18]. In the present study, systolic and diastolic blood pressures were significantly lowered by administration of

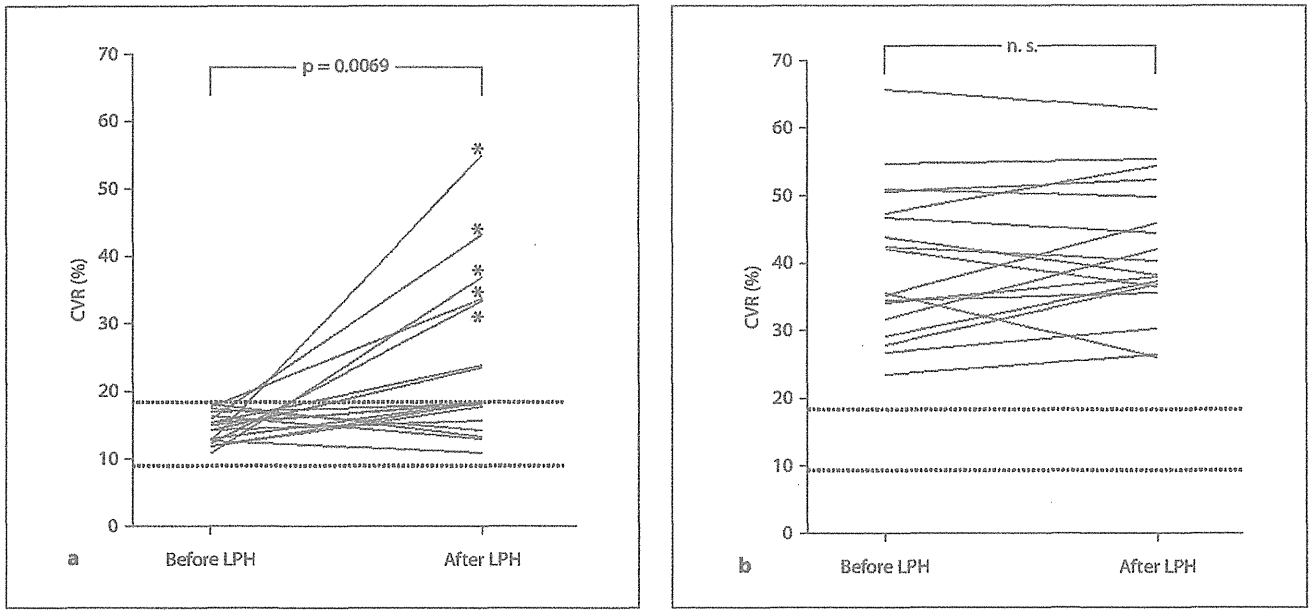

Fig. 4. Change in CVR to acetazolamide in the affected (**a**) and contralateral (**b**) MCA territories before and after initiating the administration of LPH. Upper and lower dashed horizontal lines denote mean –2SD and mean –3SD of CBF obtained in healthy volunteers, respectively. Asterisk denotes patients rated as having improved CVR.

Table 2. Factors related to improved CVR in the affected hemisphere

Factors	Improved CVR		p	
	yes (n = 5)	no (n = 13)	univariate analysis	multiple logistic regression analysis
Mean age ± SD, years	62.6 ± 5.7	60.4 ± 9.6	0.587	0.995
Male gender	5 (100%)	10 (76.9%)	0.522	0.997
Mean body mass index ± SD	24.6 ± 2.3	24.7 ± 2.3	0.882	
Current smoking	2 (40.0%)	4 (30.8%)	>0.999	
Excessive drinking	0	1 (7.7%)	>0.999	
Diabetes mellitus	1 (20.0%)	3 (23.1%)	>0.999	
Dyslipidemia	3 (60.0%)	3 (23.1%)	0.268	
Only TIA	3 (60.0%)	7 (53.8%)	>0.999	
Border zone INF	2 (40.0%)	8 (61.5%)	0.608	
ICA steno-occlusive disease	5 (100%)	6 (46.2%)	0.101	0.607
Clopidogrel	2 (40.0%)	7 (53.8%)	>0.999	
Mean difference in systolic blood pressure ± SD, mm Hg	11.8 ± 3.6	10.7 ± 4.5	0.553	
Mean difference in diastolic blood pressure ± SD, mm Hg	9.8 ± 3.9	9.8 ± 5.2	0.804	

Excessive drinking is defined as drinking alcohol >60 g/day. TIA = Transient ischemic attack; INF = infarction.

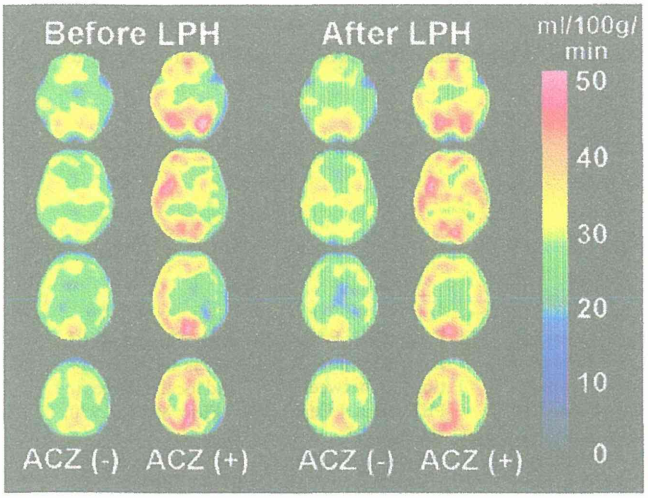

Fig. 5. Brain perfusion SPECT images of patient 3 exhibiting a reduction from 150 to 137 mm Hg in systolic blood pressure and from 94 to 79 mm Hg in diastolic blood pressure at 12 weeks after initiating the administration of LPH. CBF is slightly reduced, and CVR to acetazolamide (ACZ) is moderately reduced in the left MCA territory before LPH. While CBF remains unchanged after LPH, CVR to ACZ has improved in that region.

LPH to such patients, with average reductions of 11 mm Hg for systolic blood pressure and 10 mm Hg for diastolic blood pressure. The observations are consistent with those from a previous study [18].

While in the present study CBF did not differ between measurements before and after the administration of LPH, CVR significantly increased after the administration of LPH; 5 of the 18 patients were rated as having improved CVR, and none of the patients were rated as having deteriorated CVR. These data suggest that blood pressure-lowering therapy with LPH does apparently not result in worsening of cerebral hemodynamics within 3 months after the initiating the administration of LPH in patients with both hypertension and cerebral hemodynamic impairment due to symptomatic chronic ICA or MCA steno-occlusive disease. CVR often spontaneously improves in patients with major cerebral artery steno-occlusive disease, predominantly during the first few months after the onset of ischemic symptoms, provided no interval stroke occurs [10, 19]. This improvement is probably dependent on the development of collateral circulation [10]. The present study also showed that none of the variables, including the difference in blood pressure, were significantly associated with improved CVR. However, the absence of associations may be due to the small sample size.

In the present study, CBF and CVR did not differ between measurements taken before and after the administration of LPH in the hemisphere contralateral to the steno-occlusive artery, and all patients studied were rated as having unchanged CBF and CVR in the hemispheres. As these patients had normal CBF and CVR before the administration of LPH, the present data suggest that LPH does apparently not influence normal brain perfusion.

The present study has several limitations that require discussion. First, although the present study was an exploratory trial, statistical analysis power may be hampered by the small sample size. This is the most serious limitation. Although the prevalence of risk factors was quite different between patients with improved and unchanged CVR, no analysis was performed for statistical significance. Thus, the results of the present study are only preliminary and require confirmation in studies with larger populations. Second, patients did not receive any antihypertensive drugs within the 8 weeks after the last cerebral ischemic event and received LPH at 14 weeks after the last cerebral ischemic event. Further, only patients with moderately reduced CVR due to unilateral ICA or MCA steno-occlusive disease were enrolled in this study. Thus, the effect of LPH in an earlier phase after a cerebral ischemic event or in patients with severely reduced CVR or bilateral lesions remains unknown. Third, patients in the present study were examined for only 12 weeks after initiating the administration of LPH and for only 26 weeks after the last cerebral ischemic event. However, recurrent strokes in patients with hemodynamically compromised hemispheres generally occur during the first 6 months after the onset of ischemic symptoms [10, 19, 20]. Thus, the follow-up period in the present study may be long enough for examining the effect of LPH on brain perfusion. Finally, the comparator groups in this study may be suboptimal: confirmation of these results within a double-blind study of angiotensin receptor blocker plus thiazide diuretics versus only angiotensin receptor blocker would be of benefit.

Conclusions

Although the present study was exploratory and its results were preliminary due to the small sample size, the current data suggest that blood pressure-lowering therapy with LPH does apparently not result in worsening of cerebral hemodynamics in patients with both hyperten-

sion and cerebral hemodynamic impairment due to symptomatic chronic ICA or MCA steno-occlusive disease. Further study with larger sample sizes is needed to confirm this finding and to determine the effect of blood pressure-lowering therapy with LPH on the incidence of recurrent ischemic stroke.

Disclosure Statement

The authors declare that they have no conflict of interest to disclose.

References

1 Chobanian AV, Bakris GL, Black HR, Cushman WC, Green LA, Izzo JL Jr, Jones DW, Materson BJ, Oparil S, Wright JT Jr, Roccella EJ; the National High Blood Pressure Education Program Coordinating Committee: Seventh report of the joint national committee on prevention, detection, evaluation, and treatment of high blood pressure. Hypertension 2003;42:1206–1252.

2 Nishimura Y, Ito T, Saavedra JM: Angiotensin II AT_1 blockade normalizes cerebrovascular autoregulation and reduces cerebral ischemia in spontaneously hypertensive rats. Stroke 2000;31:2478–2486.

3 Moriwaki H, Uno H, Nagakane Y, Hayashida K, Miyashita K, Naritomi H: Losartan, an angiotensin II (AT_1) receptor antagonist, preserves cerebral blood flow in hypertensive patients with a history of stroke. J Hum Hypertens 2004;18:693–699.

4 Shah S, Khatri I, Freis ED: Mechanism of antihypertensive effects of thiazide diuretics. Am Heart J1978;95:611–618.

5 Stoltz JF, Zannad F, Kdher Y, Le Bray Des Boses B, Ghawi RE, Meilhac B, Cauchois G, Gentils M, Muller S: Influence of a calcium antagonist on blood rheology and arterial compliance in hypertension: comparison with a thiazide diuretic. Clin Hemorheol Microcirc 1999;21:201–208.

6 Araoye MA, Chang MY, Khatri IM, Freis ED: Furosemide compared with hydrochlorothiazide; long-term treatment of hypertension. JAMA 1978;240:1863–1866.

7 Calvo C, Gude F, Abellan J, Olivan J, Olmos M, Pita L, Sanz D, Sarasa J, Bueno J, Herrera J, Macias J, Sagastagoitia T, Ferro B, Vega A, Martinez J: A comparative evaluation of amlodipine and hydrochlorothiazide as monotherapy in the treatment of isolated systolic hypertension in the elderly. Clin Drug Invest 2000;19:317–326.

8 Zannad F, Bray-Desboscs L, el Ghawi R, Donner M, Thibout E, Stoltz JF: Effects of lisinopril and hydrochlorothiazide on platelet function and blood rheology in essential hypertension: a randomly allocated double-blind study. J Hypertens 1993;11:559–564.

9 Powers WJ: Cerebral hemodynamics in ischemic cerebrovascular disease. Ann Neurol 1991;29:231–240.

10 Ogasawara K, Ogawa A, Yoshimoto T: Cerebrovascular reactivity to acetazolamide and outcome in patients with symptomatic internal carotid or middle cerebral artery occlusion: a xenon-133 single-photon emission computed tomography study. Stroke 2002; 33:1857–1862.

11 Kuroda S, Houkin K, Kamiyama H, Mitsumori K, Iwasaki Y, Abe H: Long-term prognosis of medically treated patients with internal carotid or middle cerebral artery occlusion: can acetazolamide test predict it? Stroke 2001;32:2110–2116.

12 Ogasawara K, Ito H, Sasoh M, Okuguchi, Kobayashi M, Yukawa H, Terasaki K, Ogawa A: Quantitative measurement of regional cerebrovascular reactivity to acetazolamide using [^{123}I]iodoamphetamine autoradiographic method with single photon emission computed tomography: validation study using [^{15}O] H_2O positron emission tomography. J Nucl Med 2003;44:520–525.

13 Iida H, Itoh H, Nakazawa M, Hatazawa J, Nishimura H, Onishi Y, Uemura K: Quantitative mapping of regional cerebral blood flow using iodine-123-IMP and SPECT. J Nucl Med 1994;35:2019–2030.

14 Friston KJ, Frith CD, Liddle PF, Dolan RJ, Lammertsma AA, Frackowiak RS: The relationship between global and local changes in PET scans. J Cereb Blood Flow Metab 1990; 10:458–466.

15 Takeuchi R, Matsuda H, Yoshioka K, Yonekura Y: Cerebral blood flow SPET in transient global amnesia with automated ROI analysis by 3DSRT. Eur J Nucl Med Mol Imaging 2004;31:578–589.

16 Brenner BM, Cooper ME, de Zeeuw D, Keane WF, Mitch WE, Parving HH, Remuzzi G, Snapinn SM, Zhang Z, Shahinfar S; RENAAL Study Investigators: Effects of losartan on renal and cardiovascular outcomes in patients with type 2 diabetes and nephropathy. N Engl J Med 2001;345:861–869.

17 Dahlöf B, Devereux RB, Kjeldsen SE, Julius S, Beevers G, de Faire U, Fyhrquist F, Ibsen H, Kristiansson K, Lederballe-Pedersen O, Lindholm LH, Nieminen MS, Omvik P, Oparil S, Wedel H; LIFE Study Group: Cardiovascular morbidity and mortality in the Losartan Intervention For Endpoint reduction in hypertension study (LIFE): a randomised trial against atenolol. Lancet 2002; 359:995–1003.

18 Ruilope LM, Simpson RL, Toh J, Arcuri KE, Goldberg AI, Sweet CS: Controlled trial of losartan given concomitantly with different doses of hydrochlorothiazide in hypertensive patients. Blood Press 1996;5:32–40.

19 Widder B, Kleiser B, Krapf H: Course of cerebrovascular reactivity in patients with carotid artery occlusions. Stroke 1994;25:1963–1967.

20 Webster MW, Makaroun MS, Steed DL, Smith HA, Johnson DW, Yonas H: Compromised cerebral blood flow reactivity is a predictor of stroke in patients with symptomatic carotid artery occlusive disease. J Vasc Surg 1995;21:338–345.

OPEN ACCESS Freely available online

PLOS | ONE

Nicorandil Prevents $G\alpha_q$-Induced Progressive Heart Failure and Ventricular Arrhythmias in Transgenic Mice

Masamichi Hirose[1]*, Yasuchika Takeishi[2], Tsutomu Nakada[3], Hisashi Shimojo[4], Toshihide Kashihara[3], Ayako Nishio[5], Satoshi Suzuki[2], Ulrike Mende[6], Kiyoshi Matsumoto[5], Naoko Matsushita[7], Eiichi Taira[7], Fumika Sato[1], Mitsuhiko Yamada[3]

1 Department of Molecular and Cellular Pharmacology, Iwate Medical University School of Pharmaceutical Sciences, Shiwa, Iwate, Japan, 2 Department of Cardiology and Hematology, Fukushima Medical University, Fukushima, Fukushima, Japan, 3 Department of Molecular Pharmacology, Shinshu University School of Medicine, Matsumoto, Nagano, Japan, 4 Department of Pathology, Shinshu University School of Medicine, Matsumoto, Nagano, Japan, 5 The Research Center for Human and Environmental Science, Shinshu University, Matsumoto, Nagano, Japan, 6 Cardiovascular Research Center, Division of Cardiology, Rhode Island Hospital & The Alpert Medical School of Brown University, Providence, Rhode Island, United States of America, 7 Department of Pharmacology, Iwate Medical University School of Medicine, Shiwa, Iwate, Japan

Abstract

Background: Beneficial effects of nicorandil on the treatment of hypertensive heart failure (HF) and ischemic heart disease have been suggested. However, whether nicorandil has inhibitory effects on HF and ventricular arrhythmias caused by the activation of G protein alpha q ($G\alpha_q$) -coupled receptor (GPCR) signaling still remains unknown. We investigated these inhibitory effects of nicorandil in transgenic mice with transient cardiac expression of activated $G\alpha_q$ ($G\alpha_q$-TG).

Methodology/Principal Findings: Nicorandil (6 mg/kg/day) or vehicle was chronically administered to $G\alpha_q$-TG from 8 to 32 weeks of age, and all experiments were performed in mice at the age of 32 weeks. Chronic nicorandil administration prevented the severe reduction of left ventricular fractional shortening and inhibited ventricular interstitial fibrosis in $G\alpha_q$-TG. SUR-2B and SERCA2 gene expression was decreased in vehicle-treated $G\alpha_q$-TG but not in nicorandil-treated $G\alpha_q$-TG. eNOS gene expression was also increased in nicorandil-treated $G\alpha_q$-TG compared with vehicle-treated $G\alpha_q$-TG. Electrocardiogram demonstrated that premature ventricular contraction (PVC) was frequently (more than 20 beats/min) observed in 7 of 10 vehicle-treated $G\alpha_q$-TG but in none of 10 nicorandil-treated $G\alpha_q$-TG. The QT interval was significantly shorter in nicorandil-treated $G\alpha_q$-TG than vehicle-treated $G\alpha_q$-TG. Acute nicorandil administration shortened ventricular monophasic action potential duration and reduced the number of PVCs in Langendorff-perfused $G\alpha_q$-TG mouse hearts. Moreover, HMR1098, a blocker of cardiac sarcolemmal K_{ATP} channels, significantly attenuated the shortening of MAP duration induced by nicorandil in the $G\alpha_q$-TG heart.

Conclusions/Significance: These findings suggest that nicorandil can prevent the development of HF and ventricular arrhythmia caused by the activation of GPCR signaling through the shortening of the QT interval, action potential duration, the normalization of SERCA2 gene expression. Nicorandil may also improve the impaired coronary circulation during HF.

Citation: Hirose M, Takeishi Y, Nakada T, Shimojo H, Kashihara T, et al. (2012) Nicorandil Prevents $G\alpha_q$-Induced Progressive Heart Failure and Ventricular Arrhythmias in Transgenic Mice. PLoS ONE 7(12): e52667. doi:10.1371/journal.pone.0052667

Editor: Vladimir E. Bondarenko, Georgia State University, United States of America

Received June 29, 2011; **Accepted** November 19, 2012; **Published** December 20, 2012

Funding: This study was supported in part by a Grant-in-Aid for Scientific Research from Ministry of Education, Culture, Sports, Science and Technology, Japan (No. 21590276) (to MH). The funders had no role in study design, data collection and analysis, decision to publish, or preparation of the manuscript. No additional external funding received for this study.

Competing Interests: The authors have declared that no competing interests exist.

* E-mail: mhirose@iwate-med.ac.jp

Introduction

It is well known that the abnormalities in coronary hemodynamics in systolic heart failure (HF) are frequent. Myocardial oxygen demand and consumption are increased and myocardial perfusion is also impaired in HF, which can result in myocardial ischemia, necrosis and apoptosis. This is potentially a factor contributing to progressive heart failure. Nicorandil is an ATP-sensitive K^+ (K_{ATP}) channel opener and a nitric oxide donor, which dilates epicardial and resistance coronary arteries as well as peripheral resistance arterioles and systemic veins. Thus, nicorandil increases coronary blood flow, reduces preload and afterload, and exerts an antianginal action [1,2]. In addition, beneficial hemodynamic effects of nicorandil have also been demonstrated in acute HF, suggesting a possible effect of this drug in the treatment of HF [3]. In fact, intravenous administration of nicorandil attenuated exercise-induced LV diastolic dysfunction in individuals with hypertrophic cardiomyopathy, probably as a result of its beneficial effect on abnormal coronary microcirculation [4]. Moreover, chronic nicorandil administration prevented the development of HF in Dahl salt-sensitive hypertensive rats as a result of the promotion of myocardial capillary and arteriolar growth [5]. These findings support the notion that nicorandil may ameliorate HF associated with defective coronary microcirculation. Our previous study demonstrated a direct effect of nicorandil on ventricular myocardium (i.e. shortening of ventricular action

potential), leading to the prevention of ventricular tachyarrhythmias during myocardial ischemia [6].

It is known that the G protein αq-coupled receptor (GPCR) signaling pathway plays a critical role in the development of cardiac hypertrophy and HF [7–9]. Our previous study demonstrated that a transgenic mouse with transient cardiac expression of activated $G\alpha_q$ ($G\alpha_q$-TG) developed chronic HF and ventricular tachyarrhythmias [10–12]. While nicorandil may prove beneficial for the treatment of hypertensive heart failure as well as of ischemic heart disease, it remains unknown whether nicorandil has inhibitory effects on the development of HF and ventricular arrhythmias caused by activation of the G_q signaling pathway. We hypothesized that nicorandil can prevent the development of HF and HF-induced ventricular arrhythmias through improvement of coronary hemodynamics and ventricular electrophysiological property. In the present study, we investigated the inhibitory effects of nicorandil on HF and ventricular arrhythmias in $G\alpha_q$-TG mice.

Materials and Methods

The experimental protocol was approved by the institutional animal experiments committee and complied with the Guide for Care and Use of Laboratory Animals published by the US National Institutes of Health (NIH publication 85-23, revised 1996). The animal experiments were also approved by the Shinshu University School of Medicine Animal Studies Committee (approval ID 200044).

Experimental Animals

A transgenic mouse ($G\alpha_q$-TG mouse) with transient cardiac expression of activated $G\alpha_q$ was used [12]. The wild-type (WT) mice used in this study are littermates from the non-transgenic mice. The genotypes of the WT and $G\alpha_q$-TG mice were identified by polymerase chain reaction (PCR) with the use of tail genomic DNA as a template as previously reported. Our previous studies demonstrated that $G\alpha_q$-TG mice developed HF but not ventricular arrhythmias at the age of 16 weeks, whereas they developed both by 32 weeks. Therefore, to examine effects of chronic nicorandil administration on HF and ventricular arrhythmias, nicorandil (6 mg/kg/day) or vehicle was orally administered to $G\alpha_q$-TG mice from 8 to 32 weeks of age. In addition, to examine potential basal effects of long-term nicorandil treatment in WT mice, nicorandil (6 mg/kg/day) or vehicle was also administered to WT mice from 8 to 32 weeks of age. All experiments were performed in 32-week-old mice. All mice were anesthetized with sodium pentobarbital (30 mg/kg) applied intraperitoneally. The adequacy of anesthesia was monitored by watching heart rate and the frequency and the degree of motion of the sternum and of movement of the extremities.

Echocardiography

WT, nicorandil-treated WT, vehicle-treated $G\alpha_q$-TG, and nicorandil-treated $G\alpha_q$-TG female mice ($n=6$ each) were anesthetized, and cardiac function was assessed with echocardiography (GE Yokogawa Medical System, Tokyo, Japan) as previously described [13]. Hearts were viewed at the level of the papillary muscles along the short axis. In M-mode tracings, the average of three consecutive beats was used to measure the following parameters: interventricular septum thickness, left ventricular end-diastolic dimension (LVEDd), end-systolic dimension (LVESd) and fractional shortening (LVFS), which was calculated as follows: (LVEDd - LVESd)/LVEDd ×100%. Echocardiography was also performed in WT and $G\alpha_q$-TG mice at the age of 8 weeks before treatment with nicorandil.

Gross Anatomy and Histology

WT, nicorandil-treated WT, vehicle-treated Gαq-TG, and nicorandil-treated Gαq-TG female mice ($n=10$ each) were anesthetized and treated with sodium heparin (500 USP units/kg i.v.). After a midline sternal incision, hearts were quickly excised. The hearts were fixed with a 30% solution of formalin in phosphate-buffered saline at room temperature for more than 24 hours, embedded in paraffin, and then cut serially from the apex to the base. Six sections were stained with hematoxylin/eosin or Masson's trichrome for histopathological analysis. Transverse sections were captured digitally, and the cross-sectional diameter of at least 20 cardiomyocytes in each section was measured using the image analyzing software MacSCOPE (MITANI Corporation, Tokyo) on a Macintosh computer. The measurements were performed on 3 sections in each preparation and averaged. To assess the degree of fibrosis, digital microscopic images were taken from the sections stained with Masson's trichrome stain using light microscopy with a digital camera system. The measurements were performed on 3 images from different parts of the left ventricle in each preparation as described previously [14]. The fibrosis fraction was obtained by calculating the ratio of total connective area to total myocardial area from 3 images in each preparation.

Western Blot Analysis

Total protein was prepared from the ventricular myocardium of anesthetized WT, vehicle-treated $G\alpha_q$-TG and nicorandil-treated $G\alpha_q$-TG mice ($n=6$ each) using a lysis buffer (Cell Signaling Technology, Inc. Danvers, MA) to examine the protein expression of TRPC isoforms. Protein concentrations assayed, and equal amounts of the proteins were subjected to 10% SDS-PAGE and transferred to PVDF membranes. To ensure equivalent protein loading and to verify efficient protein transfer, membranes were stained with Ponceau S before incubating with primary isoform-specific antibodies against TRPC isoforms (TRPC 3 and 6; SIGMA, Saint Louis, MO) and actin [15]. Immunoreactive bands were detected with an ECL kit (Amersham Biosciences Corp., Piscataway, NJ). The densitometric intensity of bands representing TRPC isoforms was normalized to that of actin. In addition, to examine potential basal effects of long-term nicorandil treatment in WT mice, a western blot analysis was performed in vehicle-treated and nicorandil-treated WT mice ($n=5$ each).

Quantification of mRNA by Real-time PCR

Total RNA was prepared from the ventricular myocardium of anesthetized WT, vehicle-treated $G\alpha_q$-TG and nicorandil-treated $G\alpha_q$-TG mice ($n=6$ each) with Isogen (Nippon Gene Co. LTD., Tokyo, Japan) according to the manufacturer's instructions. One microgram of total RNA was used as a template for reverse transcription with the SuperScript First-Strand synthesis system for qRT-PCR (Invitrogen, Carlsbad, CA). To generate a standard curve for mRNA quantification, partial cDNA fragments of atrial natriuretic factor (ANF), B-type natriuretic peptide (BNP), β-myosin heavy chain (β-MHC), Kir6.1, Kir6.2, sulfonylurea receptor (SUR) 1, SUR2A, SUR2B, endothelial nitric oxide synthese (eNOS), inducible NOS (iNOS), connective tissue growth factor (CTGF), collagen type 1, phspholamban (PLB), sarco(endo)-plasmic reticulum Ca^{2+}-ATPase 2 (SERCA2), sodium/calcium exchanger 1 (NCX1) and acidic ribosomal protein P0 (ARPP0) were amplified from the heart cDNA by PCR with DNA polymerase Ex Taq HS (Takara Bio, Shiga, Japan) and subcloned into the pGEM-T Easy vector (Promega, Madison, WI). Real-time

PCR was performed with an ABI Prism 7900HT Sequence Detection System (Applied Biosystems, Foster City, CA). The PCR mixture (20 μl) contained FastStart Universal SYBR Green Master (Rox) (Roche Diagnostics), standard cDNA (10^2 to 10^6 ng per reaction) or 0.2 μl of reverse-transcribed cDNA samples and 100 nM of forward and reverse primers. All primers used are listed in Table S1. To choose a suitable internal control for this study, glyceraldehyde 3-phosphate dehydrogenase, β-actin, β-glucuronidase, and ARPP0 were tested, and it was found that the expression of ARPP0 mRNA was most constant between the groups. Thus, the expression of each gene was normalized to that of ARPP0 mRNA. The specificity of the method was confirmed by a dissociation analysis according to the instructions supplied by Applied Biosystems. In addition, to examine potential basal effects of long-term nicorandil treatment in WT mice, the real-time PCR was performed in WT and nicorandil-treated WT mice (n = 5 each).

Electrocardiography (ECG)

WT, nicorandil-treated WT, vehicle-treated $G\alpha_q$-TG, and nicorandil-treated $G\alpha_q$-TG female mice (n = 10 each) were anesthetized. Electrocardiography (ECG) lead II was recorded for 10 min in all mice. ECG lead II was recorded and filtered (0.1 to 300 Hz), digitized with 12-bit precision at a sampling rate of 1000 Hz per channel (Microstar Laboratories Inc., Bellevue, WA, USA), transmitted into a microcomputor and saved on CD-ROM.

Monophasic Action Potential (MAP)

WT and vehicle-treated $G\alpha_q$-TG mice were anesthetized and treated with sodium heparin (500 USP units/kg i.v.). After a midline sternal incision, hearts were quickly excised and connected to a modified Langendorff apparatus. A polyterafluoroethylene-coated silver unipolar electrode was used to stimulate the epicardial surface of the anterior left ventricle at twice the diastolic threshold current with a duration of 1 ms. A monophasic action potential (MAP) electrode was placed on the epicardial surface of the posterior left ventricle, and MAP was recorded for 10 sec at a basic cycle length of 200 ms to measure MAP duration. Each preparation was perfused under constant flow conditions with oxygenated (95% oxygen, 5% CO_2) Tyrode's solution containing in mM: NaCl, 141.0; KCl, 5.0; $CaCl_2$, 1.8; $NaHCO_3$, 25.0; $MgSO_4$, 1.0; NaH_2PO_4, 1.2; HEPES, 5; and dextrose, 5.0 (pH of 7.4 at 36±1°C). Perfusion pressure was measured with a pressure transducer (Nihon Kohden Co, Tokyo, Japan) and maintained within a pressure range (50–60 mmHg) by adjusting flow. The MAP signals were filtered (0.3 to 300 Hz), amplified (1000×) and recorded. Perfusion pressure and flow were continuously monitored during each experiment.

First, to examine direct effects of nicorandil on ventricular action potential in $G\alpha_q$-TG mouse hearts, MAP was recorded from the epicardial surface of the posterior left ventricle in vehicle-treated WT and $G\alpha_q$-TG mouse hearts (n = 8 each) before and after the application of nicorandil (1 and 10 μM). Next, to examine the mechanisms underlying the effect of nicorandil on ventricular action potential, MAP was recorded in vehicle-treated $G\alpha_q$-TG mouse hearts (n = 4) in the presence of nicorandil alone, and in the presence of nicorandil plus HMR1098 (30 μM), a blocker of cardiac sarcolemmal K_{ATP} channels.

Electrophysiological Measurement

In all mice examined, P, PR, QRS complex, QT, and RR intervals were measured from ECG lead II. The number of premature ventricular contractions (PVCs) per minute was calculated from ECG lead II. A high incidence of PVCs (High PVC) was defined as more than 20 beats/min. In MAP signals of all Langendorff hearts, automated algorithms were used to determine depolarization time relative to a single fiducial point (i.e., the stimulus). Depolarization time was defined as the point of maximal positive derivative in the action potential upstroke (dV/dt_{max}). Repolarization time was defined as the time when repolarization reached a level of 50%. MAP duration was defined as the difference between repolarization time and depolarization time.

Data Analysis

All data are shown as the mean ± SE. An analysis of variance with Bonferroni's test was used for the statistical analysis of multiple comparisons of data. Fisher's exact test was used to compare the incidence of VT between different conditions. $P<0.05$ was considered statistically significant.

Drug

Nicorandil was kindly provided by Chugai Pharmaceutical Co. (Tokyo, Japan).

Results

Nicorandil Prevented the Progression of Cardiomegaly and Contractile Dysfunction in $G\alpha_q$-TG Mice

To evaluate whether chronic administration of nicorandil could prevent the progression of HF in $G\alpha_q$-TG mice, cardiac morphology was examined in WT, nicorandil-treated WT, vehicle-treated $G\alpha_q$-TG and nicorandil-treated $G\alpha_q$-TG mice at the age of 32 weeks. Gross examination of the four-chamber section of the heart revealed all chambers to be dilated in the vehicle-treated $G\alpha_q$-TG heart compared with WT and nicorandil-treated Gαq-TG hearts (Fig. 1A). The vehicle-treated $G\alpha_q$-TG mouse exhibited marked cardiomegaly. The heart/body weight ratio increased in vehicle-treated $G\alpha_q$-TG mice compared with WT mice, but nicorandil significantly reduced the ratio in $G\alpha_q$-TG mice (Table 1). The left atrial size/tibial length ratio was also increased in vehicle-treated $G\alpha_q$-TG compared with WT hearts. Nicorandil decreased the ratio in $G\alpha_q$-TG hearts (Table 1). Echocardiography was performed, and representative M-mode echocardiograms are shown in Figure 1B. Compared with the WT mice, vehicle-treated $G\alpha_q$-TG mice exhibited impaired left ventricular contractility and chamber dilation as demonstrated by the markedly reduced LVFS and the increased LVEDd (Fig. 1B and Table 2). However echocardiographic parameters such as reduced LVFS and increased LVEDd were significantly improved in nicorandil-treated $G\alpha_q$-TG compared with vehicle-treated $G\alpha_q$-TG mice (Fig. 1B and Table 2). Moreover, LVEDd and LVFS age-dependently changed in $G\alpha_q$-TG mice, whereas the values in nicorandil-treated $G\alpha_q$-TG mice at 32 weeks were similar to those at 8 weeks, indicating that nicorandil prevented the progression of cardiomegaly and contractile dysfunction in $G\alpha_q$-TG mice (Fig. 1C).

Nicorandil Inhibited Myocardial Fibrosis but not the mRNA Expression of Profibrotic Genes and Cardiomyocyte Hypertrophy in $G\alpha_q$-TG Mice

We examined the effects of chronic nicorandil administration on left ventricular myocardial fibrosis and cardiomyocyte hypertrophy in WT, vehicle-treated $G\alpha_q$-TG and nicorandil-treated $G\alpha_q$-TG mice at the age of 32 weeks. Extensive interstitial fibrosis in the left ventricle was observed in vehicle-treated $G\alpha_q$-TG hearts compared with WT and nicorandil-treated $G\alpha_q$-TG hearts

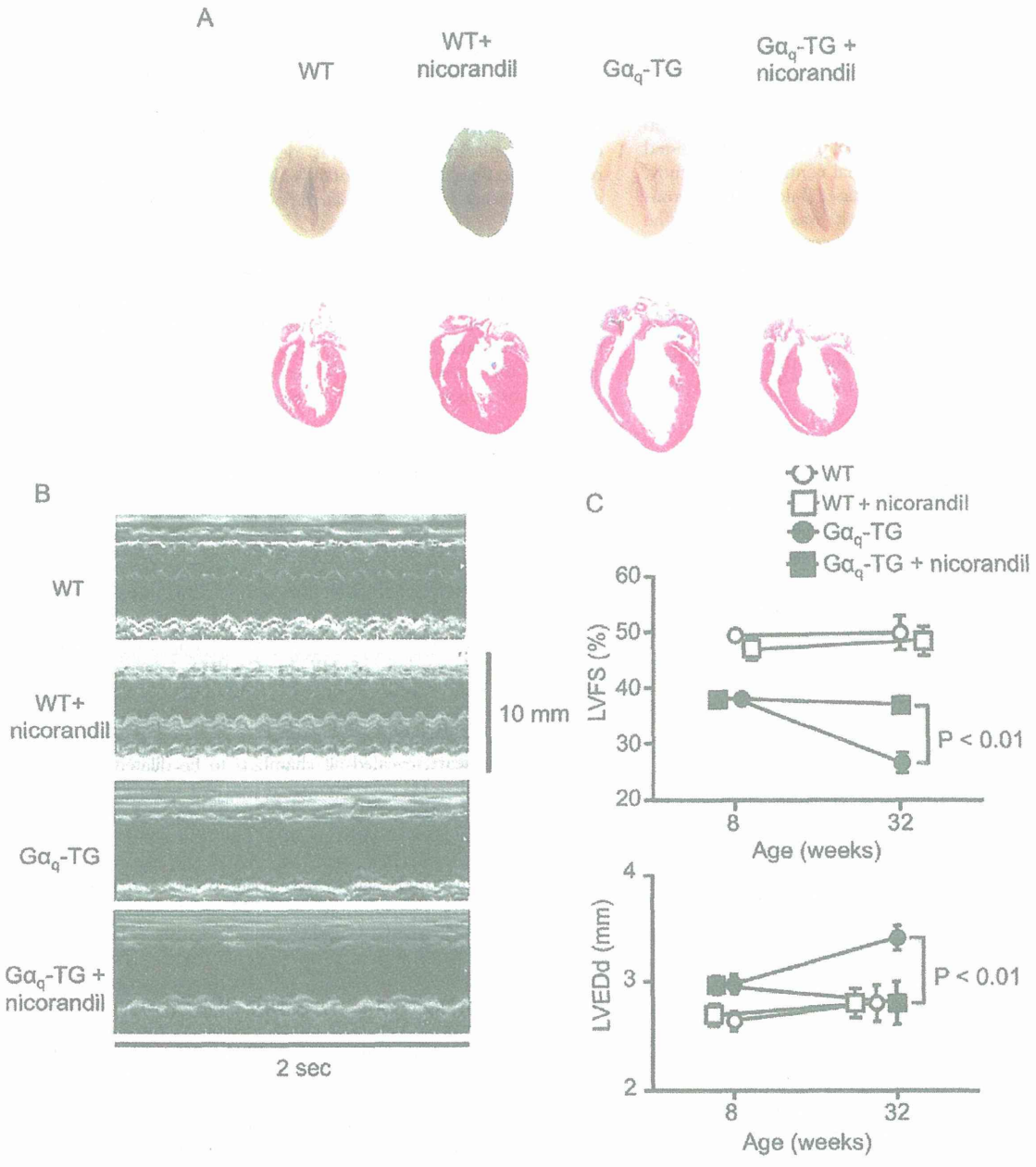

Figure 1. Effects of nicorandil on cardiac morphology and on the left ventricular contractile function. Panel A: Gross examination of the four-chamber section of a heart and its histology stained with hematoxylin/eosin in a WT (wild-type), WT+nicorandil, $G\alpha_q$-TG, and $G\alpha_q$TG+nicorandil mouse heart. Original magnification: 1.25×. Panel B: Representative M-mode echocardiograms of a WT, WT+nicorandil, $G\alpha_q$-TG, and $G\alpha_q$TG+nicorandil mouse at the age of 32 weeks. Panel C: Age-dependent changes in left ventricular fractional shortening (LVFS) and left ventricular end-diastolic dimension (LVEDd) in WT, WT+nicorandil, $G\alpha_q$-TG, and $G\alpha_q$TG+nicorandil mice. WT+nicorandil, nicorandil-treated WT; $G\alpha_q$-TG, vehicle-treated $G\alpha_q$-TG; $G\alpha_q$TG+nicorandil, nicorandil-treated $G\alpha_q$TG. Mice at age of the 32 weeks were used.
doi:10.1371/journal.pone.0052667.g001

(Fig. 2A). The degree of myocardial fibrosis in the left ventricle was significantly greater in vehicle-treated $G\alpha_q$-TG mice than in WT mice (Fig. 2B). Nicorandil significantly reduced the increased interstitial fibrosis in the left ventricle of $G\alpha_q$-TG mice (Fig. 2B). We next examined the expression of profibrotic genes, such as the genes for CTGF and collagen type 1, to investigate whether these morphological observations were accompanied by alterations in gene expression relevant to fibrotic changes. The expression of CTGF and collagen type 1 was significantly upregulated in $G\alpha_q$-TG hearts compared with WT mouse hearts (Fig. 2C). In nicorandil-treated $G\alpha_q$-TG hearts, the gene expression of CTGF and collagen type 1 was similar to that in vehicle-treated $G\alpha_q$-TG hearts (Fig. 2C).

Table 1. General parameters and the incidence of premature ventricular contraction (PVC) in WT, WT+nicorandil, $G\alpha_q$-TG, and $G\alpha_q$-TG+nicorandil mice.

Parameters	WT	WT+nicorandil	$G\alpha_q$-TG	$G\alpha_q$-TG+nicorandil
BW (g)	29.8±1.5	24.2±0.3[b]	29.8±1.4	29.7±1.2
HW (mg)	130±2.4	125±4.0	170±8.8[b]	148±9.5[+]
HW/BW (mg/g)	4.4±0.2	5.1±0.2	5.8±3[a]	5.0±0.5
LA/TL (mm/mm)	0.14±0.01	0.17±0.01	0.27±0.02[b]	0.21±0.02[b,+]
PVC	1/10	0/10	9/10[b]	3/10[+]
PVC (>20 beats/min)	0/10	0/10	7/10[b]	0/10[$]

Data are the mean ± SE obtained from 10 mice for each group. [a]p<0.05, [b]p<0.01 vs. WT, +p<0.05, [$]p<0.01 vs. values in corresponding parameters of $G\alpha_q$-TG.
doi:10.1371/journal.pone.0052667.t001

Microscopic observation revealed that the cross-sectional diameter of cardiomyocytes was profoundly increased in vehicle-treated $G\alpha_q$-TG mice compared with WT mice (Fig. 2D). The increase cross-sectional diameter was not attenuated in nicorandil-treated $G\alpha_q$-TG mice (Fig. 2D).

Nicorandil did not Inhibit Fetal Gene Expression and TRPC Channel Protein Levels in $G\alpha_q$-TG Mice

We next examined the mRNA expression of fetal type genes such as ANF, β-MHC and BNP in WT, vehicle-treated $G\alpha_q$-TG and nicorandil-treated $G\alpha_q$-TG mice at the age of 32 weeks. Expression of ANF, BNP and β-MHC was significantly upregulated in $G\alpha_q$-TG hearts compared with WT mouse hearts (Fig. 3A). In nicorandil-treated $G\alpha_q$ -TG hearts, the gene expression of ANF, BNP, and β-MHC was similar to that in vehicle-treated $G\alpha_q$-TG hearts (Fig. 3A). A recent study suggested that the activation of TRPC channels participated in the generation of cardiac hypertrophy [16]. Moreover, the protein levels of TRPC3 and 6 were increased in $G\alpha_q$-TG mouse hearts [11]. Therefore, we examined effects of nicorandil on the protein expression of TRPC channel subtypes in $G\alpha_q$-TG hearts. The levels of TRPC 3 and 6 channels were significantly increased in $G\alpha_q$-TG hearts compared with WT hearts (Fig. 3B). The expression of TRPC 3 and 6 was not significantly different between vehicle-treated $G\alpha_q$-TG and nicorandil-treated $G\alpha_q$-TG mouse hearts (Fig. 3B).

Gene Expression of ATP-sensitive K^+ (K_{ATP}) Channel Subunit, Nitric Oxide Synthase (NOS), and Ca^{2+}-handling Proteins

We examined the mRNA expression of ATP-sensitive K^+ (K-ATP) channel subunits such as Kir 6.1, Kir 6.2, SUR1, SUR2A and SUR2B in WT, vehicle-treated $G\alpha_q$-TG and nicorandil-treated $G\alpha_q$-TG mice at the age of 32 weeks. The expression of Kir 6.2, SUR2A, and SUR2B was significantly downregulated in vehicle-treated $G\alpha_q$-TG mouse hearts compared with that in WT mouse hearts (Fig. 4). Interestingly in nicorandil-treated $G\alpha_q$-TG hearts, the gene expression of SUR2B but not Kir 6.2 or SUR2A was similar to that in WT hearts (Fig. 4). Previous study has shown that nicorandil upregulates eNOS expression in rat hearts with myocardial infarction [17]. We also examined the mRNA expression of eNOS and iNOS in WT, vehicle-treated $G\alpha_q$-TG and nicorandil-treated $G\alpha_q$-TG mice at 32 weeks of age. The mRNA expression of eNOS was significantly increased in nicorandil-treated $G\alpha_q$-TG hearts compared with vehicle-treated $G\alpha_q$-TG hearts (Fig. 4). Next, we examined the mRNA expression of PLB, SERCA2, and NCX1 in WT, vehicle-treated $G\alpha_q$-TG and nicorandil-treated $G\alpha_q$-TG mouse hearts at the age of 32 weeks. The expression of PLB and SERCA2 was significantly downregulated in vehicle-treated $G\alpha_q$-TG hearts compared with that in WT mouse hearts (Fig. 5). Interestingly in nicorandil-treated $G\alpha_q$-TG hearts, the gene expression of SERCA2 but not PLB was similar to that in WT hearts (Fig. 5). In contrast to the expression of PLB and SERCA2, NCX1 expression was similar among WT, vehicle-treated $G\alpha_q$-TG and nicorandil-treated $G\alpha_q$-TG mouse hearts.

Nicorandil Reduces the Number of Premature Ventricular Contractions (PVCs) in $G\alpha_q$-TG Mice

ECG lead II was recorded for 10 min in anesthetized WT, vehicle-treated $G\alpha_q$-TG and nicorandil-treated $G\alpha_q$-TG mice. Shown in Figure 6 are representative ECGs. The upper 2 cases show ventricular arrhythmias recorded from vehicle-treated $G\alpha_q$-TG mice: in case 1, PVC was frequently observed; in case 2, the ECG demonstrated consecutive ventricular beats, which are features of VT. In contrast, the lower 3 cases recorded from a WT, nicorandil-treated WT, $G\alpha_q$-TG, and nicorandil-treated $G\alpha_q$-TG mouse showed P waves and QRS complexes with regular RR intervals without any arrhythmia, indicating a sinus rhythm. Table 1 shows the overall data for ventricular arrhythmias.

Table 2. Echocardiographic parameters in WT, WT+nicorandil, $G\alpha_q$-TG, and $G\alpha_q$-TG+nicorandil mice.

Parameters	WT	WT+nicorandil	$G\alpha_q$-TG	$G\alpha_q$-TG+nicorandil
IVS (mm)	0.76±0.05	0.68±0.03	0.55±0.04[b]	0.62±0.07[a]
LVEDd (mm)	2.8±0.12	2.8±0.07	3.4±0.12 [b]	2.8±0.16[$]
LVFS (%)	49.8±2.9	47.0±1.4	26.7±1.6	37.0±0.9[b, $]

Data are the mean ± SE obtained from 6 mice for each group. [a]p<0.05, [b]p<0.01 vs. WT, +p<0.05, [$]p<0.01 vs. values in corresponding parameters of $G\alpha_q$-TG. LVEDd, left ventricular end-diastolic dimension; IVS, intraventricular septum.
doi:10.1371/journal.pone.0052667.t002

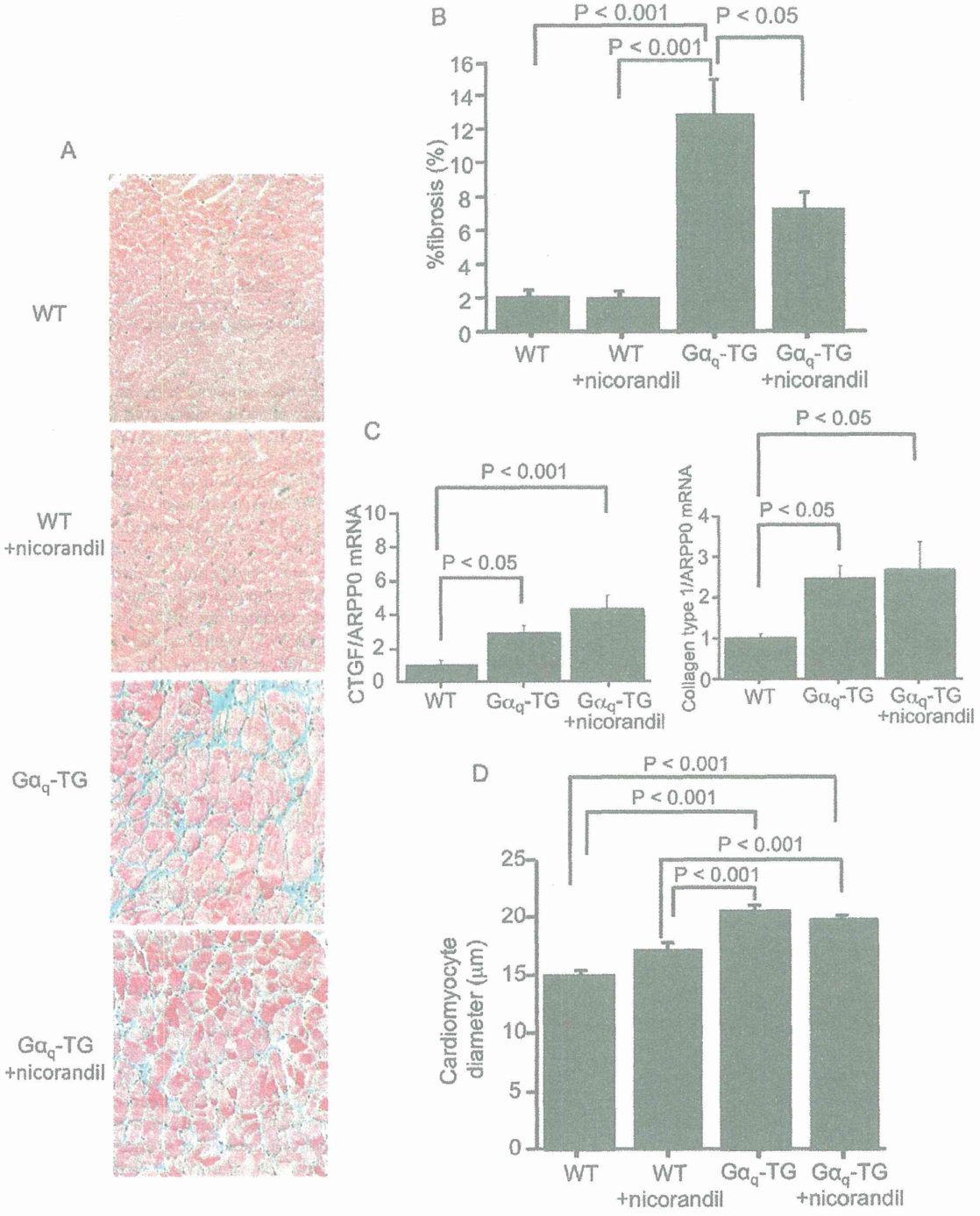

Figure 2. Effects of nicorandil on the left ventricular fibrosis and on connective tissue growth factor (CTGF) and collagen type 1 gene expression. Panel A: Histology of the left ventricle stained with Masson's trichrome in a WT, WT+nicorandil, $G\alpha_q$-TG, and $G\alpha_q$TG+nicorandil mouse. Original magnification: 40×. Panel B: Comparison of the fibrosis fraction in the left ventricle in WT, WT+nicorandil, $G\alpha_q$-TG, and $G\alpha_q$TG+nicorandil mice. Panel C: Quantitative analyses of CTGF and collagen type 1 gene expression by real-time real-time reverse transcriptase-polymerase chain reaction (RT-PCR) in WT, $G\alpha_q$-TG and $G\alpha_q$-TG+nicorandil hearts. Data for CTGF and collagen type 1 were normalized to those for ARPP0. Data are the mean ± SE obtained from 6 mice for each group. Panel D: Comparison of cardiomyocyte size in the left ventricle in WT, WT+nicorandil, $G\alpha_q$-TG, and $G\alpha_q$TG+nicorandil mice.
doi:10.1371/journal.pone.0052667.g002

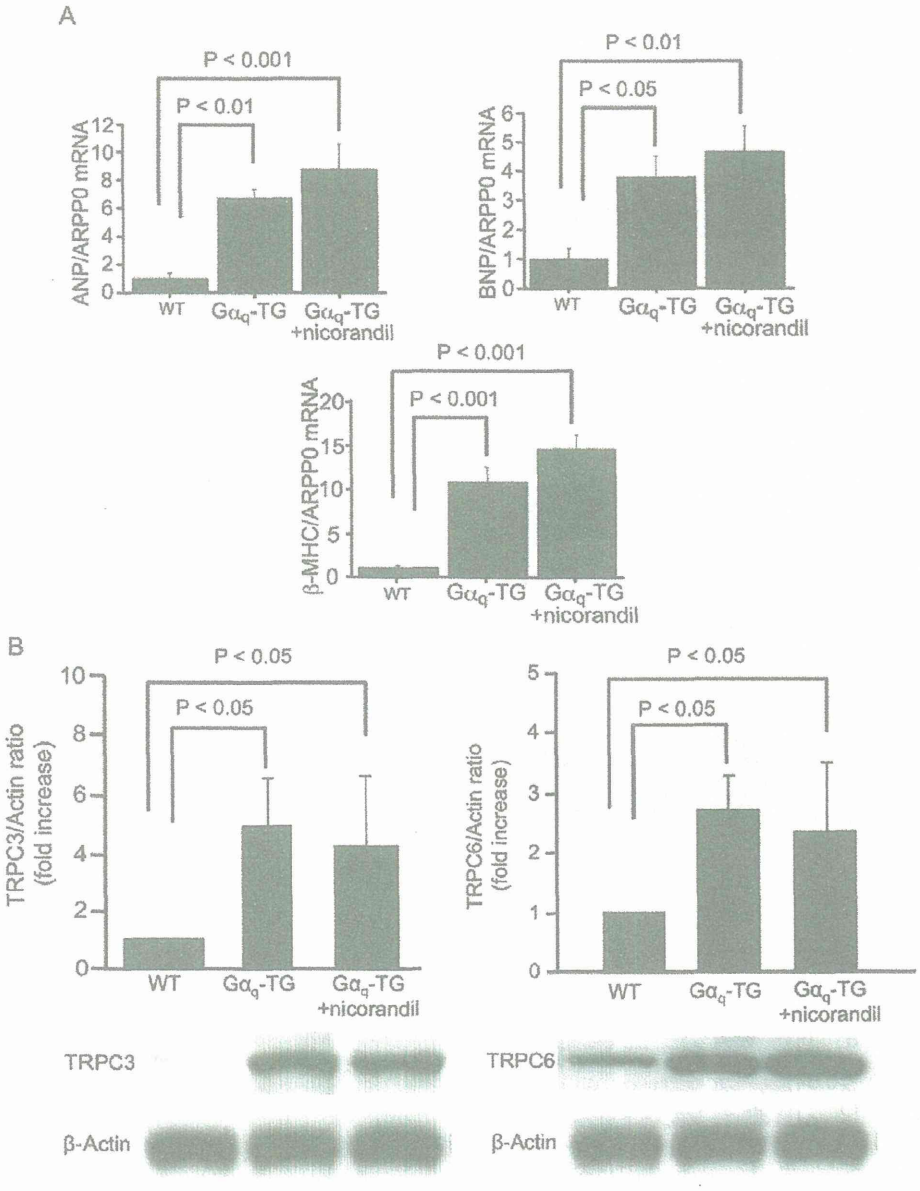

Figure 3. Effects of nicorandil on ANP, BNP, and β-MHC gene expressions and on protein expression of canonical transient receptor potential (TRPC) channel isoforms. Panel A: Quantitative analyses of ANP, BNP, and β-MHC gene expression by real-time RT-PCR in WT, $G\alpha_q$-TG and $G\alpha_q$-TG+nicorandil hearts. Data for ANP, BNP, and β-MHC were normalized to those for ARPP0. Data are the mean ± SE obtained from 6 mice for each group. Panel B: Expression of TRPC channel isoforms in WT, $G\alpha_q$-TG and $G\alpha_q$-TG+nicorandil hearts. TRPC isoform expression was normalized to actin expression and expressed relative to wt (set at 1). Data are the mean ± SE obtained from 6 mice for each group. ANF, atrial natriuretic factor; BNP, B-type natriuretic peptide; β-MHC, β-myosin heavy chain; ARPP0, acidic ribosomal protein P0. Mice at the age of 32 weeks were used.
doi:10.1371/journal.pone.0052667.g003

Ventricular arrhythmias such as a high PVC count (more than 20 beats/min) were not observed in WT and nicorandil-treated WT mice. In contrast, a high number of PVCs was observed in 7 of 10 vehicle-treated $G\alpha_q$-TG mice (Table 1). Interestingly, a high PVC count was not observed in any nicorandil-treated $G\alpha_q$-TG mice tested, indicating a significant reduction of ventricular arrhythmias in nicorandil-treated $G\alpha_q$-TG mice compared with vehicle-treated $G\alpha_q$-TG mice.

Nicorandil Restores the Baseline Values of P and QT Intervals in $G\alpha_q$-TG Mice

Table 3 shows overall data for the electrophysiological parameters in WT, nicorandil-treated WT, vehicle-treated $G\alpha_q$-TG and nicorandil-treated $G\alpha_q$-TG mice at 32 weeks of age. All ECG parameters were longer in vehicle-treated $G\alpha_q$-TG mice than WT mice. Interestingly, while the PR and RR interval was still prolonged in nicorandil-treated $G\alpha_q$-TG mice compared with WT mice, the P interval and QT interval were restored to the

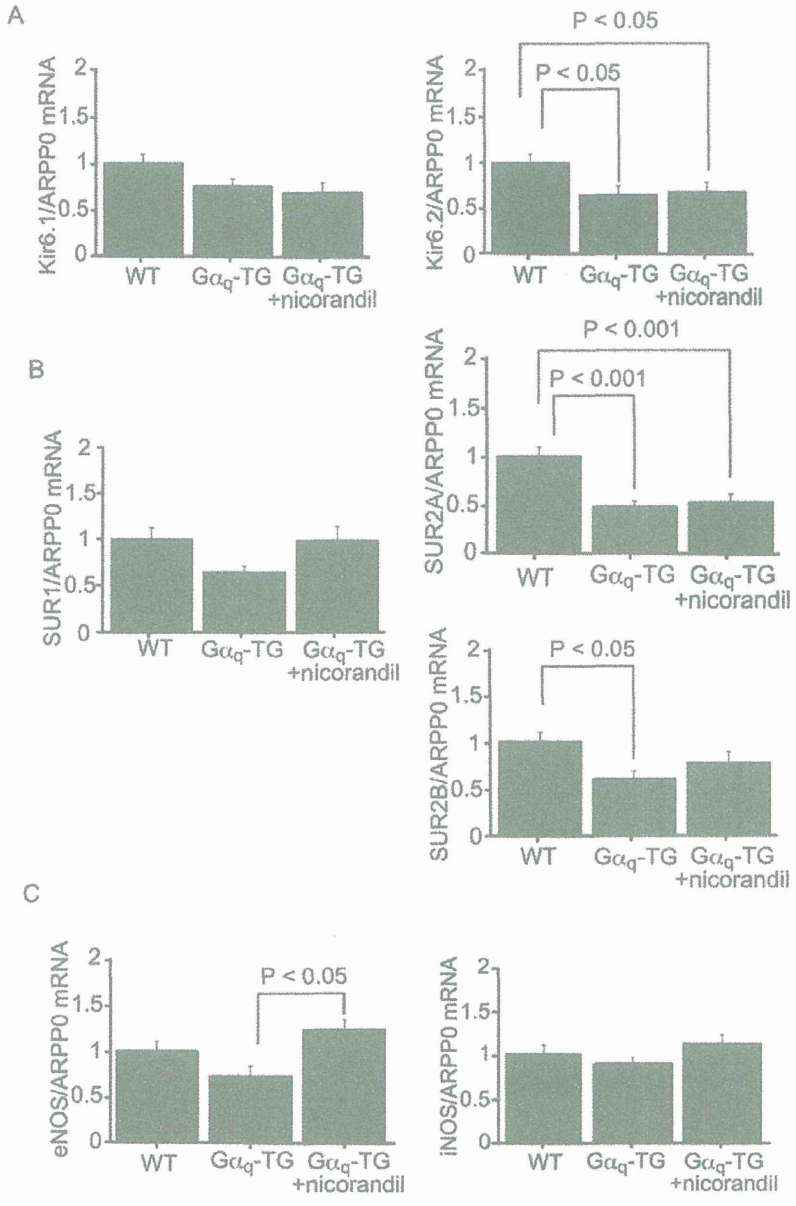

Figure 4. Quantitative analyses of Kir6.1 (A), Kir6.2 (A), SUR1 (B), SUR2A (B), SUR2B (B), eNOS (C), and iNOS (C) gene expression by real-time RT-PCR in WT, $G\alpha_q$-TG and $G\alpha_q$-TG+nicorandil hearts. Data for Kir6.1, Kir6.2, SUR1, SUR2A, SUR2B, eNOS, and iNOS were normalized to those for ARPP0. Data are the mean ± SE obtained from 6 mice for each group. SUR1, sulfonylurea receptor 1; SUR2A, sulfonylurea receptor 2A; SUR2B, sulfonylurea receptor 2B; eNOS, endothelial nitric oxide synthase; iNOS, inducible nitric oxide synthase; ARPP0, acidic ribosomal protein P0. Mice at the age of 32 weeks were used.
doi:10.1371/journal.pone.0052667.g004

normal level in nicorandil-treated $G\alpha_q$-TG compared with vehicle-treated $G\alpha_q$-TG mice.

Acute Application of Nicorandil Shortens the Prolonged Left Ventricular MAP Duration and Prevents Ventricular Tachyarrhythmias in $G\alpha_q$-TG Mice

Shown in Figure 7A are representative examples of ventricular MAPs recorded from the posterior left ventricle in Langendorff-perfused WT and $G\alpha_q$-TG hearts at the age of 32 weeks during steady state pacing at a cycle length of 200 msec. Ventricular MAP duration was prolonged in the $G\alpha_q$-TG heart compared with the WT heart before acute nicorandil administration. After the nicorandil treatment, MAP duration shortened in the $G\alpha_q$-TG heart but not WT heart (Fig. 7A). In addition, from the pooled data (Fig. 7B), nicorandil (1 and 10 μM) significantly shortened ventricular MAP duration in $G\alpha_q$-TG hearts but not in WT hearts. Moreover, HMR1098 significantly attenuated the shortening of MAP duration induced by nicorandil in the $G\alpha_q$-TG heart (Fig. 7C). Shown in Figure 7D are representative examples

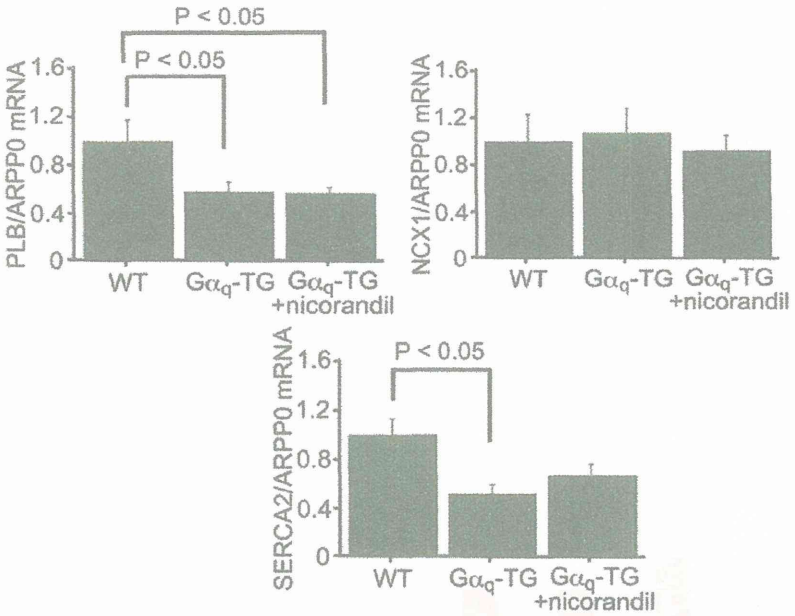

Figure 5. Quantitative analyses of PLB, SERCA2, and NCX1 gene expression by real-time RT-PCR in WT, $G\alpha_q$-TG and $G\alpha_q$-TG+nicorandil hearts. Data for PLB, SERCA2, and NCX1 were normalized to those for ARPP0. Data are the mean ± SE obtained from 6 mice for each group. PLB, phospholamban; NCX1, sodium/calcium exchanger 1; ARPP0, acidic ribosomal protein P0. Mice at the age of 32 weeks were used.
doi:10.1371/journal.pone.0052667.g005

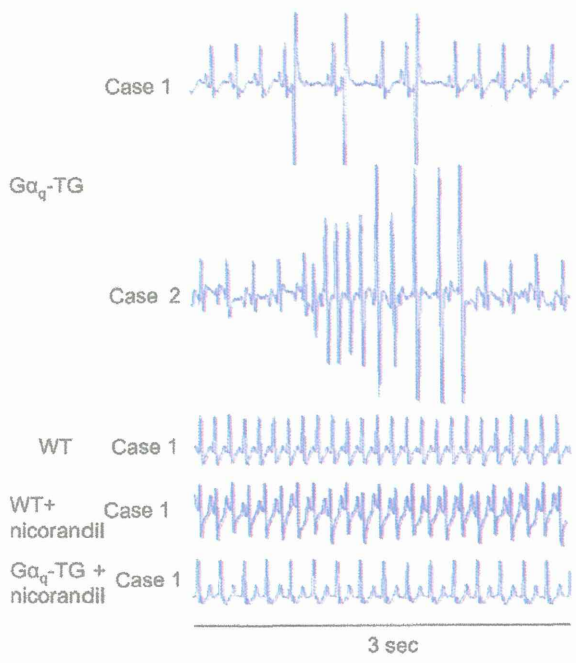

Figure 6. ECG lead II recordings from WT, WT+nicorandil, $G\alpha_q$-TG, and $G\alpha_q$+nicorandil mice. The upper 2 ECGs show premature ventricular contraction (PVC) and ventricular repetitive beats in anesthetized $G\alpha_q$-TG mice. The lower 3 ECGs recorded from a WT, WT+nicorandil, and $G\alpha_q$-TG+nicorandil mouse show P wave and QRS complex with a regular RR interval without any arrhythmia, indicating sinus rhythm. Mice at the age of 32 weeks were used. See text for details.
doi:10.1371/journal.pone.0052667.g006

of ventricular repetitive beats in the Langendorff-perfued $G\alpha_q$-TG heart during spontaneous sinus rhythm before and after acute nicorandil administration. PVC and ventricular repetitive beats were frequently observed in the $G\alpha_q$-TG heart before nicorandil was administered (Fig. 7D, top). After the nicorandil treatment, MAP duration was shortened, and PVC and repetitive ventricular beats were not induced in the $G\alpha_q$-TG heart (Fig. 7D, middle and bottom). High PVC was observed in 6 of 8 Langendorff-perfused $G\alpha_q$-TG hearts before nicorandil treatment but only 1 of 8 $G\alpha_q$-TG hearts after ($p<0.05$).

Effects of Long-term Treatment with Nicorandil on WT Mouse Hearts

Chronic nicorandil treatment from 8 to 32 weeks of age had no effect on electrical and contractile function, hypertrophy, fibrosis, (Figs. 1, 2, 6, and Tables 1, 2, and 3). Figure 8 shows overall data for several genes and TRPC protein expression in WT and nicorandil-treated WT hearts. The chronic nicorandil treatment had no effect on gene and protein expression in WT mouse hearts (Fig. 8).

Discussion

In this study, we found that chronic administration of nicorandil for 24 weeks prevented the progression of heart failure and ventricular arrhythmia in $G\alpha_q$-TG mice. We also found that nicorandil inhibited ventricular interstitial fibrosis, attenuated the decreased SUR2B gene expression, and attenuated or prevented the decrease of eNOS and SERCA2 in $G\alpha_q$-TG mouse hearts. It has been suggested that abnormalities in coronary hemodynamics in systolic heart failure contribute to ventricular remodeling, myocardial dysfunction and progressive heart failure. Both endothelium-dependent and -independent mechanisms of coronary vasodilatation are impaired in heart failure [18–20]. For

Table 3. Electrocardiographic parameters in WT, WT+nicorandil, $G\alpha_q$-TG, and $G\alpha_q$-TG+nicorandil mice.

Parameters	WT	WT+nicorandil	$G\alpha_q$-TG	$G\alpha_q$-TG+nicorandil
P (msec)	18±1	16±1	25±1[b]	22±1[+]
RR (msec)	142±5	166±10	186±9 [b]	193±16 [b]
PR (msec)	39±3	43±2	62±3 [b]	55±5 [b]
QRS (msec)	16±0.5	15±0.5	19±1[a]	17±2
QT (msec)	34±2	32±2	43±2[b]	34±3[+]

Data are the mean ± SE obtained from 6 mice for each group. [a]p<0.05, [b]p<0.01 vs. WT, +p<0.05 vs. values in corresponding parameters of vehicle-treated $G\alpha_q$-TG.
doi:10.1371/journal.pone.0052667.t003

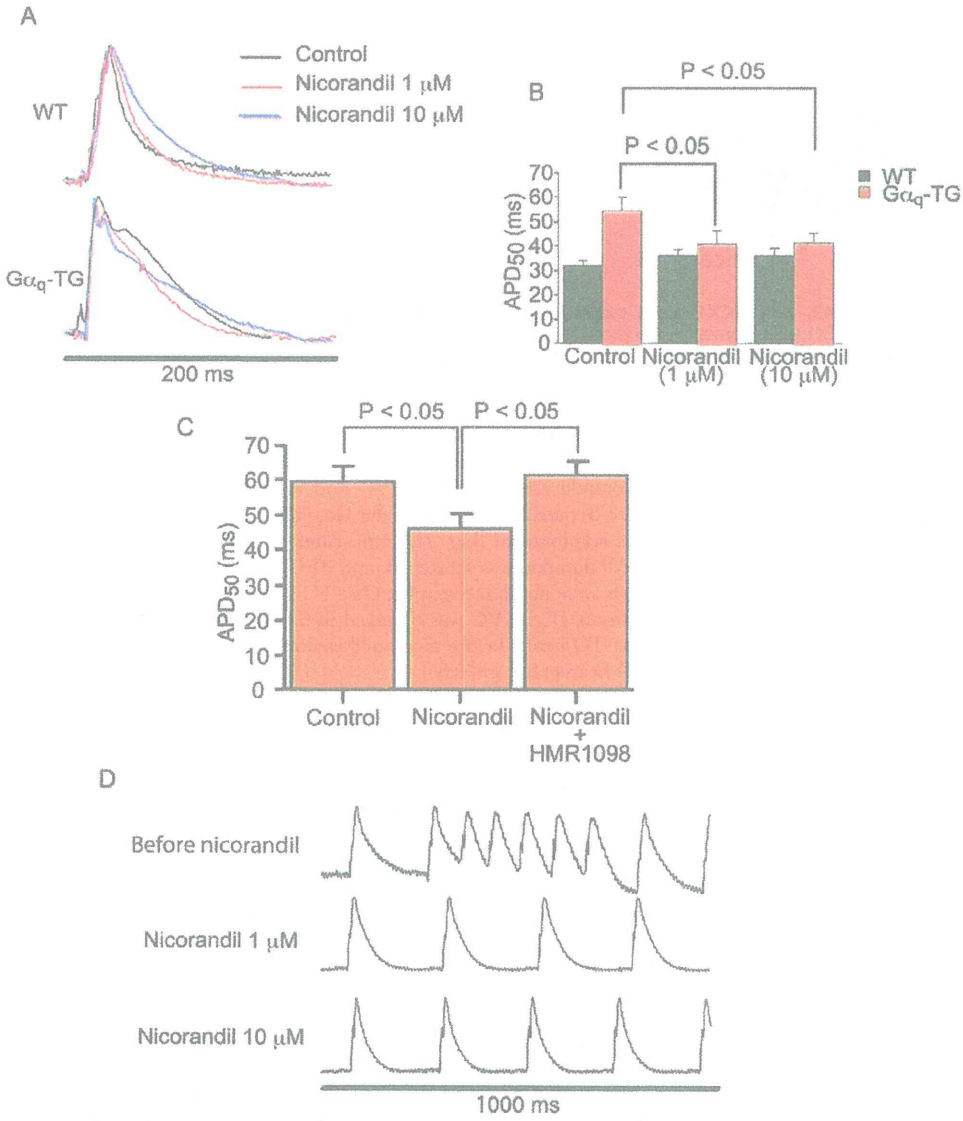

Figure 7. Effects of nicorandil on the ventricular action potential duration and spontaneous premature ventricular beats. Panel A: Representative examples of monophasic action potentials (MAPs) recorded from the posterior left ventricle in a Langendorff-perfused WT and $G\alpha_q$-TG heart during steady state pacing at a cycle length of 200 msec. Panel B: Overall data for MAP duration in WT and $G\alpha_q$-TG hearts before and after acute nicorandil administration. Panel C: Overall data for MAP duration in $G\alpha_q$-TG hearts during the control, in the presence of nicorandil (10 μM) alone, and in the presence of nicorandil plus HMR1098 (30 μM), a blocker of cardiac sarcolemmal K_{ATP} channels. Panel D: Spontaneous premature ventricular beats in a Langendorff-perfused $G\alpha_q$-TG heart before and after acute nicorandil administration. Mice at the age of 32 weeks were used. See text for details.
doi:10.1371/journal.pone.0052667.g007